

**THE DEVELOPMENT OF SCRATCH TEST METHODOLOGY AND
CHARACTERIZATION OF SURFACE DAMAGE OF
POLYPROPYLENE**

A Thesis

by

MIN HAO WONG

Submitted to the Office of Graduate Studies of
Texas A&M University
in partial fulfillment of the requirements for the degree of

MASTER OF SCIENCE

August 2003

Major Subject: Mechanical Engineering

**THE DEVELOPMENT OF SCRATCH TEST METHODOLOGY AND
CHARACTERIZATION OF SURFACE DAMAGE OF
POLYPROPYLENE**

A Thesis

by

MIN HAO WONG

Submitted to Texas A&M University
in partial fulfillment of the requirements
for the degree of

MASTER OF SCIENCE

Approved as to style and content by:

Hung- Jue Sue
(Chair of Committee)

Terry Creasy
(member)

David E. Bergbreiter
(member)

Dennis L. O'Neal
(Head of Department)

August 2003

Major Subject: Mechanical Engineering

ABSTRACT

The Development of Scratch Test Methodology and Characterization of Surface Damage of Polypropylene. (August 2003)

Min Hao Wong, B.S., Nanyang Technological University

Chair of Advisory Committee: Dr. Hung-Jue Sue

A new scratch test methodology is proposed. The new test methodology is developed based on the principles of materials science and solid mechanics, which include the consideration of material parameters, use of microscopy for image analysis and the finite element method (FEM). The consistency and reproducibility of test results are shown using a new scratch test device on two sets of neat and talc-filled polypropylene (PP) systems. Three different test conditions, *i.e.*, linear load increase under constant rate, constant load under constant rate, and linear rate increase under constant load, have been conducted to determine the most effective, informative test conditions for evaluation of scratch resistance of polymers. Experimental observations and FEM results show a good qualitative correlation. The unique advantages of the new scratch test method for evaluating scratch resistance of polymers are discussed. A systematic study of surface damage effected by a progressive scratching load is performed on model polypropylene (PP) systems. Mar-scratch and stress-whitening transitions can be readily observed, and the corresponding critical loads determined. Distinctive scratch hardnesses and surface damage features are found for different material systems. Visibility of scratched surface is quantified using gray level analysis *via* a flatbed scanner and a commercial image analysis tool. It is found that the onset of scratch visibility can be determined accurately and reproducibly using the custom-built scratcher under progressive loading condition. Talc particles are found to be responsible for the increased light scattering, leading to greatly increased visibility. The observed scratch visibility is also found to be related to the measured frictional force profiles. Approaches for producing scratch resistant PP are discussed.

In loving memory of my mother,

Madam Har Nui Cheh

ACKNOWLEDGMENTS

I would like to give my most sincere thanks to Dr Hung-Jue Sue, who has provided me with this unique opportunity to learn under him. My experience here as a graduate student has been very rewarding because of his knowledge, experience and patience. I would also like to thank the sponsors who helped fund this research—the Texas A&M Scratch Behavior Consortium (Advanced Composites - Brian Coleman, BP Chemical - Kathryn Shuler, Luzenac - Richard Clark, Solvay Engineered Polymers - Edmund Lau, Visteon - Beth Wichterman and Rose Ryntz), the State of Texas (ARP #32191-73130) and Defense Logistic Agency (SP0103-02-D-0003) in this research endeavor. Special thanks are also given to the Society of Plastics Engineers - South Texas Section and Fred Lee of Atlas Materials Testing Technology for their generous donation and loan of equipment for this research. I would like to thank my fellow colleagues and friends, Goy Teck Lim, David Yuntao Li, Jongil Weon, Dr. Jim Lu, Allan Moyse, Patrick Rood, Jennifer Garcia-Meitin, Masaya Kotaki, Gam Ki Tak and many others who had helped me along in my research.

This work is dedicated to my mother who passed away the Christmas before this thesis was written. She will always be my strength and reason that will see me through hard times.

TABLE OF CONTENTS

	Page
ABSTRACT.....	iii
DEDICATION.....	iv
ACKNOWLEDGMENTS.....	v
TABLE OF CONTENTS.....	vi
LIST OF TABLES.....	viii
LIST OF FIGURES.....	ix
 CHAPTER	
I INTRODUCTION.....	1
1.1 Background.....	1
1.2 Scratch Test Methodologies.....	2
1.3 Characterization of Surface Damage due to Scratch in Polymers.....	3
1.4 Objectives of Research.....	4
1.5 Overview of Research.....	5
II AN OVERVIEW OF SCRATCH.....	6
2.1 Introduction.....	6
2.2 Theory of Scratch.....	6
2.3 Classification of Scratch Tests.....	10
2.4 Summary.....	16
III EVALUATION AND QUANTIFICATION OF SCRATCH.....	17
3.1 Introduction.....	17
3.2 The Surface Phenomena of Scratch.....	17
3.3 The Visibility of Scratch.....	20
3.3.1 VIEEW [®]	22
3.4 Issues Concerning Evaluation and Quantification of Scratch.....	23
3.5 Summary.....	24

CHAPTER	Page	
IV	A NEW SCRATCH TEST METHODOLOGY FOR POLYMERS.....	26
	4.1 Introduction.....	26
	4.2 Experimental.....	26
	4.2.1 Custom-Built Scratch Test Device.....	26
	4.2.2 Model Material System and Test Procedures.....	30
	4.2.3 Evaluation of Scratch Damage.....	31
	4.3 Finite Element Analysis.....	32
	4.4 Results and Discussion.....	33
	4.4.1 Experimental Results.....	33
	4.4.2 Repeatability.....	43
	4.4.3 Numerical Analysis Findings.....	43
	4.5 Conclusions.....	45
V	STUDY OF SURFACE DAMAGE OF POLY- PROPYLENE UNDER PROGRESSIVE LOAD.....	47
	5.1 Introduction.....	47
	5.2 Experimental.....	48
	5.2.1 Experimental Approach and Materials.....	48
	5.2.2 Quantification of Scratch Damage.....	48
	5.3 Results and Discussion.....	49
	5.3.1 Homopolymer Surface Features.....	49
	5.3.2 Scratch Hardness.....	58
	5.3.3 Homopolymer Frictional Force Profile.....	61
	5.3.4 Copolymer Surface Features.....	63
	5.3.5 Copolymer Frictional Force Profile.....	69
	5.3.6 Scratch Visibility.....	72
	5.3.6.1 Stress-whitening.....	72
	5.3.6.2 Ductile vs. Brittle Failure.....	77
	5.4 Conclusions.....	78
VI	CONCLUSIONS.....	79
	6.1 Summary.....	79
	6.2 Recommendations for Future Research.....	80
	REFERENCES.....	82
	VITA.....	89

LIST OF TABLES

TABLE		Page
2.1	Mohs' hardness scale.....	11
3.1	List of definitions of hardness.....	19
3.2	Comparison of various techniques used in evaluation of scratch....	25
4.1	Comparison of functionalities of different scratch devices.....	29
4.2	Suggested tests for scratch characterization.....	30
4.3	Composition of PP systems.....	30
4.4	Mar-scratch transition values.....	40
5.1	Significant parameters of highlighted regions in Figures 5.2 & 5.3.	53
5.2	Mechanical properties of PP systems.....	54
5.3	Skin-core depths of PP.....	56
5.4	Scratch hardness obtained from graphical method.....	59

LIST OF FIGURES

FIGURE		Page
2.1	Schematic of the scratching process.....	7
3.1	Schematic of light-scattering measuring apparatus (Kody et al.[28]).....	21
4.1	Design of the custom-built scratch test device. (a) Schematic of the spring-loaded scratch tip. (b) Schematic of control system of scratch unit and data acquisition unit.....	28
4.2	(a) Definitions of scratch widths and scratch depths (b) Actual cross section of a scratch groove.....	33
4.3	Comparison of (a) experimental and (b) FEA results....	34
4.4	Talc-filled copolymers scratched under different conditions. (a) Linear load increase and constant speed, (b) constant speed and load and (c) linear rate increase and constant load.....	36
4.5	Scratch widths and depths from linear load increase test condition on four different model PP systems.....	36
4.6	SEM of talc-filled homopolymer scratched under Test A conditions.....	37
4.7	Variation of scratch depth along scratch groove in talc- filled copolymer.....	37
4.8	Variation of scratch width with normal load.....	38
4.9	Mar-scratch damage transition of (a) homopolymer and (b) talc-filled homo-polymer in Test <i>A</i>	38

FIGURE	Page	
4.10	Scanned image showing scratch damage transition in a talc-filled homopolymer under Test A conditions. (a) Entire scratch length, (b), (c) and (d) are enlarged details showing transition in scratch damage.....	41
4.11	Normal load profile of neat PP under linear load increase test during scratch.....	42
4.12	Percentage standard deviation for scratch widths and depths in the linear load increase test.....	42
4.13	von Mises stress distribution for different load cases (after Lim [52]).....	44
4.14	von Mises stress distribution for different load cases, cross-section view (after Lim [52]).....	44
5.1	Gray level plot of scratch groove from scanner image.....	47
5.2	(a) Scanned image of scratched homopolymer, (b) region 1, (c) region 2, (d) region 3, (e) region 4 and (f) region 5 are SEM micrographs of highlighted regions in the scratch groove. Note that that region 5 shows fibril breakage after sonication.....	51
5.3	(a) Scanned image of scratched talc-filled homopolymer, (b) region 1, (c) region 2, (d) region 3, (e) region 4 and (f) region 5 are SEM micrographs of highlighted regions in the scratch groove. Note that that region 5 shows fibril breakage after sonication.....	52
5.4	Scratch width of regions shown in Figure 5.2 & 5.3. Spikes denote stick-slip events.....	56

FIGURE	Page
5.5 Skin-core morphology of (a) homopolymer, (b) talc-filled homopolymer, (c) copolymer and (d) talc-filled copolymer. Note that the cross-section of scratch groove on each surface corresponds to that at 30N normal load.....	57
5.6 Graphical method of obtaining scratch hardness.....	59
5.7 Frictional force profile from scratch test of (a) homopolymer and (b) talc-filled homopolymer.....	60
5.8 Frictional force profile of PC showing constant slope in both curves.....	62
5.9 (a) Scanned image of scratched copolymer that was sonicated, (b) region 1 and (c) region 2 shows extensive deformation indicated by box.....	64
5.10 (a) Scanned image of scratched talc-filled copolymer that was sonicated, (b) region 1 and (c) region 2.....	65
5.11 Inter-pit distance shows an increase against scratch distance.....	66
5.12 Fibrils in (a) homopolymer and (b) talc-filled homopolymer.....	68
5.13 Engineering stress-strain graph of a material that yields and cold-draws. (after McCrum et al. [74]).....	69
5.14 Frictional force profile from scratch test of (a) copolymer and, (b) talc-filled copolymer, (c) shows the detailed profile of (b) that corresponds to Figure 5.10(b).....	70

FIGURE		Page
5.15	SEM micrograph of exposed talc particles in a talc-filled homopolymer. Arrow indicates scratch direction.....	71
5.16	(a) Image from VIEEW [®] , white region indicates stress-whitening, (b) frictional profile for this talc-filled copolymer specimen, dashed line shows excellent correlation with onset of stress-whitening.....	74
5.17	Critical load to onset of stress-whitening.....	74
5.18	Area of scratch groove that was stress-whitened.....	75
5.19	Gray level plot of scanned image of a copolymer <i>via</i> flatbed scanner.....	75

CHAPTER I

INTRODUCTION

1.1 Background

Scratch deformation of polymeric surfaces has become an important area of research in the field of materials science and mechanics. The use of polymers in an ever widening range of products has brought attention to the ability of the polymers to withstand damages during service life. Electronics components, such as notebook casings and compact discs, to automotive parts, such as car interior instrument panels and console modules to lenses and paint coatings are some applications where polymers act as a physical protection from whatever damage that daily use will entail. Being low cost and light-weight, and having the capability to be molded into desired shapes and surface textures, it is not surprising to find that polymers are rapidly replacing, or being used with metals in many applications. With the growing demands for low cost thermoplastic olefins (TPO), researchers now face new challenges to ensure the satisfactory performance of the polymeric products. The resistance of polymers to surface damage is one such challenge.

This thesis follows the style of *Wear*.

1.2 Scratch Test Methodologies

There are a variety of ways and methods to perform scratch resistance evaluation on polymers. Depending on the issues of concern, a given test method designed to evaluate scratch resistance based on scratch hardness, tangential hardness, scratch visibility, wear and deformation mechanisms. Although most scratch tests have been developed for metals and ceramics, these tests cannot be applied to polymers without some modifications. This is mainly because of the differences in mechanical behaviors between metals/ceramics and polymers, where viscoelastic effects are significant.

Due to the lack of a standard for scratch tests, many companies have to come up with their own version of scratch tests. Often the tests are limited in scope and only pay attention to one material characteristic, or give a relative ranking of hardness. Some examples are the Mohs' mineral hardness test, which is used by gemologists in comparing the relative hardness of minerals. Another test uses a range of pencils from 6B to 9H. The hardest pencil lead that does not leave a scratch groove is recorded. A crockmeter tests the ability of paints or colorings to adhere to textile by rubbing it with a stylus. Both methods are popular in the paint and coatings industry because of their simplicity. A more systematic method that is popular among automotive-related companies is the Ford five-finger test. This method employs stainless steel styli to scratch TPOs that are mainly used in the interior of a car and to determine its ranking of scratch resistance.

Scientists and researchers prefer a more rigorous approach in determining scratch resistance. Although a few commercial products are available, many of them prefer to design and build their own apparatus. The numerous factors that can influence scratch imply that different scratch experiments have to be designed in order to investigate the appropriate factor(s). Using different geometry, such as cone, ball, pyramidal tips, or flat punch will generate scratch patterns that are often difficult to compare among one another. Other factors, such as size, speed, normal load, temperature and lubrication,

compound to the complexity of the problem. Ideally, all of the abovementioned factors should be controlled tightly to generate reproducible data. In practice, different devices are built which have vastly different capabilities. As a result, test data are not always comparable. Hence, the main objective of this research is to propose a standardized test, which has sufficient flexibility to accommodate a range of test conditions, the relevant factors will be easily controlled, and because of the identical setup, there is a basis of comparison.

1.3 Characterization of Surface Damage due to Scratch in Polymers

Current efforts in studying scratch are mainly focused on observing the types of phenomena that occurs under changing conditions. An example might be varying the conical angle of a cone-shaped tip and noting the type of scratch damage produced. The results provide a general understanding in how the severity of damage is dependent on different conical angle. Yet, this does not enhance significantly our ability to predict the type of damages, which may occur in different scratch conditions. The severity of scratch damage in polymers is related to the failure mode of the polymeric surface under a given test condition. Whether the polymeric surface undergoes ironing, ductile drawing, brittle cracking, machining or fragmentation, it will be intricately linked to the degree of physical damage, *i.e.*, the depth and width of the scratch groove. Other effects, such as melting due to surface heat generation and filler debonding, may also occur. The key in predicting scratch damage phenomena is to quantify scratch damage. Development in this area is still in its infancy, partly due to the lack of a standardized test method. Thus, another major objective of this research is to provide a means of quantifying scratch.

To accurately measure the amount of deformation that occurs during scratch is not as straightforward as it seems. The width of scratch can be measured easily during

or in the aftermath of scratching. However, the depth is a more difficult issue. Expensive and sophisticated equipment, such as profilometers, depth sensing equipment, and scanning probe microscopes, are required to measure depth.

Scratch visibility is gaining more importance because of demands for aesthetics for many applications. Scratch visibility is a quality obvious to any human eyes but difficult to quantify in the laboratory. The main reason why the perception of scratch visibility differs from person to person is because it is affected by both environmental (light intensities, angle, surface roughness) and human (different sensitivities to wavelength and surface texture) factors. In spite of this, many attempts have been made to quantify visibility by measuring the differences in light reflectance of the surface. This method has had limited success so far, mainly because the relationship between the results obtained and human perception of scratch is still unclear. It is hoped that this research will enable an establishment of a test method that allows the quantification of scratch resistance via both the physical surface damage dimensions approach and the scratch visibility approach.

1.4 Objectives of Research

The objective of this study is to devise a new methodology to investigate surface damage of polymers. This study will focus on developing a set of appropriate procedures and conditions of the scratch test. The results from different procedures will be examined and the optimal procedure will be selected. The surface damage from the selected procedures will be studied in detail. Direct experimental observations and measurements based on frictional force, geometrical measurements and scratch visibility will be devised and assessed. The ultimate goal of this research is to propose a comprehensive methodology that will address many of the concerns in industry and

academia on scratch of polymers by producing reliable and reproducible test data for quantitative evaluation of scratch resistance.

1.5 Overview of Research

A brief review of the theory of scratch will be given in Chapter II. It will also include a review of past and present methods used in the study of scratch. Chapter III gives a review on the quantification techniques employed in assessing scratch damage and visibility.

The basics of the new scratch apparatus built specifically for this research will be explained in Chapter IV. The methods and results from using different test conditions will also be presented in the same chapter. Discussion for the selection of the best test method will also be given.

New analytical tools in the evaluation of scratch will be used in Chapter V. The methods employed will include analyzing frictional profile during scratch, scratch visibility and surface study of the scratch groove. Different materials will be tested to characterize their scratch behavior. Methods on improving scratch resistance will also be discussed.

CHAPTER II

AN OVERVIEW OF SCRATCH

2.1 Introduction

In this chapter, the definition of scratch will be introduced along with the fundamental theory of scratch. A brief review of the scratch tests currently available will follow.

2.2 Theory of Scratch

When a hard object is placed in contact on a surface and moves across the surface, a scratch groove is created (Figure 2.1). This process is termed *scratching*. Scratch is a part of *tribology*, which is defined as “the science and technology of interacting surfaces in relative motion”. It involves the study of friction, wear and lubrication [1]. There are two quantities, friction and hardness, which are often linked to scratch. Friction may be understood as the resistance encountered when one body moves over another. In sliding friction, the sliding coefficient of friction, μ , is defined as

$$\mu = \frac{F}{W} \quad (2.1)$$

where F is the tangential force required to move the body over the counterface and W is the normal load. The value of μ of polymeric surfaces can range from 0.06 for PTFE (polytetrafluoroethylene) to larger than 2 in rubbers [2].

Many materials are found to obey the three Laws of Friction, which may be stated as follows:

1. the friction force is proportional to the normal load.
2. the friction force is independent of the apparent area of contact.
3. the friction force is independent of the sliding velocity.

The reliability of these three Laws of Friction is not consistent. It is often only applicable in a limited range of test conditions and differs greatly for different materials. However, the three laws do provide useful generalizations of empirical observations. Polymers often do not follow the First and Second Laws, because of its viscoelastic behavior and indentation softness. Further explanations on how the three Laws arise can be found in the monograph by Hutchings [1].

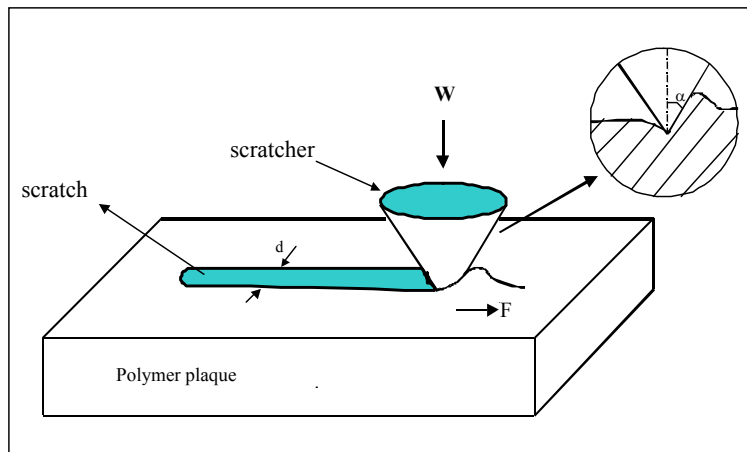


Figure 2.1: Schematic of a scratching process.

The contributions to friction can be classified under two categories, i.e, friction due to adhesion, F_{adh} , and deformation, F_{def} . The adhesion contribution arises from the molecular attractive forces that operate at the asperities that exist on each surface. These asperities are the tiniest points that provide the actual contact between surfaces. In polymers, the strength of adhesion will depend on the size of the asperities and chemical groups present in the polymer chain. The size of the asperities will determine whether van der Waals or capillary forces dominate [3]. Secondary bonds formed through hydrogen bonding and van der Waals forces will also contribute to the polymer adhesion. The strength of the bonds formed will vary according to the chemical structure of the polymer; generally polar molecules will produce the larger adhesion forces.

The deformation term comes from any process that deforms the surface and dissipates energy while sliding over it. In polymers, the two major contributions are plastic deformation and viscoelastic deformation. An asperity can be modeled as a conical point with semi-angle α . A tangential force, often taken to be the shear strength of the softer material, will be required to slide the conical asperity across the surface, thus causing the plastic deformation. The coefficient of friction that arises will be:

$$\frac{F_{plastic}}{W} = \mu = \left(\frac{2}{\pi}\right) \cot \alpha \quad \text{conical asperity} \quad (2.2)$$

$$\frac{F_{plastic}}{W} = \mu = \cot \alpha \quad \text{wedge asperity}$$

The wedge asperity form of equation is used in a plane strain model, where the asperity is taken to be a wedge of semi-angle α .

In a viscoelastic material, energy will be dissipated as heat during viscoelastic deformation. The energy dissipated per unit distance during this process will contribute to friction. If a cylindrical roller of radius R , is rolled over the viscoelastic material

under normal load W , the deformation can be isolated to include viscoelastic deformation only. The frictional force $F_{viscoelastic}$ is given as:

$$F_{viscoelastic} = 0.17\beta W^{4/3} R^{-2/3} (1-\nu^2)^{1/3} E^{-1/3} \quad (2.3)$$

Here ν is Poisson's ratio, E is the real part of Young's modulus, β is the fraction of the total energy that is dissipated.

In an indentation hardness test where a spherical indenter is applied under constant load on to a smooth surface of a perfectly plastic material, the Meyer hardness is defined as the ratio of the load, W , to the projected area of the indentation. Thus, if d is the diameter of depression left behind after the indenter has lifted away from the surface, the Meyer hardness is given as [4]:

$$H_M = \frac{4W}{\pi d^2} \quad (2.4)$$

This relationship is true even for indenters of conical or pyramidal geometry. For metals and ceramics, hardness and depth are found to obey the following relationship

$$W = kd^n \quad (2.5)$$

which is known as Meyer's law. k and n are constants to be found for the material being studied, while W and d has the usual meaning. The value of n generally exceeds 2 and for many materials it is found to lie between 2 to 2.5. Many authors have found that $n = 2$ for glassy polymers such as poly (methyl methacrylate) (PMMA) [5,6] and polystyrene (PS) [7]. Similar results were also found for semicrystalline polymers such as PP [8].

Scratch hardness is defined as the normal load of the indenter over the load bearing area. It is normally taken to be equivalent to the indentation mean pressure p_m exerted on the material during scratch. For a viscoelastic-plastic material, such as polymers, elastic recovery is almost instantaneous and the load bearing area can be approximated as a circle with its diameter the same as the scratch width. Thus scratch hardness H_s can be defined as

$$H_s = \frac{4W}{\pi d^2} \quad (2.6)$$

Notice that it has identical form to the Meyer hardness defined earlier. It was also argued by Briscoe et al. [9] that viscoelastic recovery of polymers does not affect scratch width significantly. Thus it is reasonable to measure the scratch width after the test to obtain scratch hardness.

The ratio of tangential force, F , over the normal load, W , is herein defined as the scratching coefficient of friction, μ_{sc} [10]

$$\mu_{sc} = \frac{F}{W} \quad (2.7)$$

This is to distinguish the parameter obtained using this test method as opposed to the coefficient of friction normally found by the sliding of two planar surfaces, mentioned in earlier paragraphs.

There are a number of other hardness values which are also used by researchers to quantify scratch-related hardness; these will be discussed briefly in the next chapter, although they will not be used in this work.

2.3 Classification of Scratch Tests

Over the years, numerous scratch test devices have been built commercially or custom-built by researchers to study scratch responses of polymers at various length scales. In the following sections, a brief description of each test will be given. The range and functionality of each type of test will be mentioned.

It is generally recognized that there are two types of surface damage – *mar* and *scratch*. A *mar* is a mark caused by a sliding body that is too shallow to be perceived by the casual human eyes alone but nevertheless does become visible when present in large quantities. A good example is the typical damage found on sand-abraded paint coats. A *scratch* is a mark that forms visible grooves and/or surface damage; this is the typical damage mode for surfaces that withstand heavy moving loads by swivels, ball bearings, etc. Many tests exist today that characterizes *mar*, *scratch* or both. A detailed overview

of these test methods found in the open literature and over the web is presented below. It should be understood that despite the attempt to be as comprehensive as possible, there are probably many more scratch test methods that are not covered here. In general, the numerous scratch machines that were designed can be classified into the type of scratch tests being conducted; (A) single-stylus scratch test, (B) multiple-stylus scratch test, (C) pendulum sclerometer test, (D) pin-on-disc test and (E) nanoscratch test.

- A. Single-stylus scratch test— this method employs a single stylus to slide over the polymer surface. The geometry of the stylus tip is commonly spherical and conical, uncommon tips such as knife edges and screwdriver blades are also used.
- B. Mohs' hardness test [4,11]. The Mohs' hardness test for minerals has been used since 1822. If a solid is able to scratch the surface of a selected mineral, it will have the same hardness rating as that mineral. The hardness scale simply consists of 10 minerals arranged in order from 1 to 10. Diamond is rated as the hardest and is indexed as 10; talc as the softest with index number 1. Each mineral in the scale will scratch all those below it as shown in Table 2.1. This method is not of much use to the materials engineer as the scale is not evenly space and polymers will occupy the lower range.

Table 2.1. Mohs' hardness scale

Mineral	Mohs' Hardness Scale
Diamond	10
Corundum	9
Topaz	8
Quartz	7
Orthoclase (Feldspar)	6
Apatite	5
Fluorite	4
Calcite	3
Gypsum	2
Talc	1

- Pencil hardness test [12,13]. Similar to the Mohs' hardness test and adopted by the paint and coating industries, the pencil hardness test is used to evaluate the scratch resistance of coatings. Pencil leads of various hardnesses (6B – 9H) are pushed across the surface of specimens at an angle of 45° . The hardest pencil lead that does not break and does not leave any scratch mark gives the scratch resistance rating of the specimens.
- Needle test [14]. On a tensile testing machine, Ramsteiner et al. installed a fixture where a needle with a conical tip is attached at one end. As the tensile machine moves vertically with a speed of 0.083 mm/s, the needle makes vertical scratches on the specimens. The normal load for the scratches is controlled by weights in the range of 0.1 – 1.1 N and the needles used had included angles of 60° , 97° and 120° .
- Scratching machine by Briscoe et al. [15-18]. The scratching machine consists of a rigid, adjustable but non-moving arm that houses the indenter. Specimens are placed on a moving stage whose motion is controlled by a computer. Piezoelectric force transducers are installed at the indenter holder to record the frictional forces and a heating cell has been incorporated to carry out tests at various temperatures. Dead weights are placed on the conical and spherical indenters to impose normal loads onto the specimens. The scratch rates used range from 0.001 to 40 mm/s.
- Scratch Apparatus by Gauthier and Schirrer [19]. Using an Instron tensile test machine and a commercial servo mechanism, the scratch apparatus consists of a temperature-controlled (-70 to 120°C) box containing the samples and moving tips. An external computer is used to control the motion of the tips and to record the normal and tangential loads, speeds of tips and temperatures of the tests. The constant normal load can range from 0.05 to 5 N and the scratch rates can be increased in step-size from 0.01 to 100 mm/s within the same scratch pass. Conical diamond indenter was used with a spherical tip of 20 – 400 μm in diameter.

- Scratch test rig by Wang et al. [20]. The test rig built can perform tests using normal loads from 1 to 100 N, either applied constantly or linearly increased over the scratch length and at constant scratch rates ranging from 1 to 200 mm/s. Data like the normal and tangential loads and indentation depth are acquired using the digital output to the computer and a heated stage was included for tests at elevated temperatures. Diamond conical tip (of 120° included angle), steel spherical tip of 1 mm in diameter and 0.8-mm chisel-point tip were used.
 - In-house scratch test apparatus by Ni and Faou [21]. The in-house scratch apparatus can perform scratch tests with loads from 1 – 8 N, in intervals of 1 N and at constant scratch rates of 0.011 – 0.46 mm/s. Sapphire and diamond spherical indenters with diameters of 0.15 and 1.168 mm were adopted for their study.
 - Revetest scratch tester [22,23]. This commercially built scratch test device can perform several modes of scratch tests including frictional-force-controlled and penetration-depth-controlled. Optical microscope objectives are mounted on the machine to scan pre- and post-scratch profiles with a software package to provide real-time data display. The load range (both normal and frictional) of the machine is from 1 to 200 N and the scratch rate is from 0.003 to 6.667 mm/s. The machine is also capable of carrying out progressive load (0.01 – 30 N) and multi-pass scratch tests using Vickers, Knoop and spherical indenters
- B. Multiple-stylus test— this is a variation of the single stylus method. The Ford five-finger test is a representative example.
- Ford five-finger test [24-27]. Used widely in the automotive industry, the test is used to evaluate the scratch visibility on a scale of 1 to 5, with higher values indicating more surface damages. Up to five spherical scratch tips of 1 or 7 mm can be used for testing and the normal dead load can vary from 0.6 to 20 N by adding weight plates. The rate at which the scratches are made is controlled by a compressed air pump and is approximately 100 mm/s. This method gives a

relative ranking on the damage formed during scratch but does not quantify nor identify any critical values.

C. Pin-on-disc test— the Taber pin-on-disc wear test is a commonly used method in determining the wear properties of a material. However some researchers have modified it to perform scratch tests instead of wear tests.

- Taber test & Pin-on-disc machine [28,29]. Kody and Martin [28] adopted the Teledyne-Taber shear/scratch tester in their study to examine the scratch damage of talc-filled polypropylene. Placed on a rotating base, flat samples are scratched by a conical diamond tip attached at the end of a cantilever arm, along which weight can be adjusted from 0 to 10 N. The conical tip has an included angle of 90° and a diameter of $152 \mu\text{m}$ at its point and the scratch rate used was 1.8 mm/s. For the study of Chanda et al. [29], they employed a similar pin-on-disc machine and used a load range of 10 – 40 N and scratch rates of 1.04 – 2.08 m/s.
- Scratch resistance testing machine [30]. This device consists of conical diamond stylus of radius $15 \mu\text{m}$ and 60° angle with a rotary stage. The normal load is supplied via a hydraulic setup using water as mass. The specimen is mounted on the stage and rotated at a constant rate. The stylus scratches either in a spiral or concentric manner. Scratch tests can be done under increasing load or constant. Typical load range is 0 – 60 g, sample diameter is 50 – 70 mm.

D. Pendulum Sclerometer—this method uses a pendulum to slide against the surface of the specimen.

- Single-pass pendulum sclerometer [31-34]. The pendulum machine comprises of a rigid swinging bar that is pivoted at one end with an indenter or disc blade and dead weights attached at the other end. By releasing the free end of the bar from a height, scratches are made on the test specimens at the lowest point of the swinging trajectory. The length and depth of the scratches can be adjusted by

moving the machine stage where the test specimens are secured. The indenters used are conical in shape with various included angles (30° to 120°) and with tips of $6 - 14 \mu\text{m}$ in diameter. Disc blades of 30 mm in diameter and different included angles (30° to 120°) were also used in their study. The calculation of the normal load applied will be much more complicated and the scratch groove formed is different from that of the above two methods.

- E. Nanoscratch test— this category of scratch tests is defined by the scale of damage formed during scratch. An instrument such as the atomic force microscope (AFM) [35-38] is used to produce scratches with widths in the sub-micron to nanometer range. Scratch damage features exhibit very different behavior compared to those formed using the tests mentioned earlier. This test is relevant in probing the micro- and nanoscale surface damage behavior of polymers
- Scratch tester by Jardret et al. [39]. Unlike other scratch test devices that carry out load-controlled tests, this scratch tester built can perform displacement-controlled scratch tests. Scratches are made on the specimens by the movement of the indenter and a piezoelectric transducer is installed next to the indenter to record all the forces. In their study, Berkovich indenters had been used. There are also other customized test machines built by researchers for their work [40-43].
 - Commercial instruments— Micro and Nano Scratch Testers [44,45], Nano Indenter[®] XP [46], Nano Indenter[®] XPW [47] and Triboindenter[®] [48,49]
 - Scanning probe microscopy (SPM) instruments— the advent of atomic force microscopes has given researchers the ability to manipulate objects at the nanoscale. They have become a popular method for researchers to conduct nanoscratch experiments [35-38]. Related instruments such as the point contact microscope and the frictional force microscope [36] are also used in nanoscratch experiments.

2.4 Summary

The basic theory of scratch is presented here. Two key concepts are introduced, which are friction and hardness of scratch. It will be seen later that these two quantities provide a valuable means to characterize scratch damage and resistance.

The review of scratch test devices for the macroscopic testing presented clearly reveals that the ranges of normal loads and scratch rates for most devices are rather limited while some of them may only be good for the evaluation of mar studies and thus insufficient for scratch studies. All the current test devices reviewed cannot judiciously determine the exact scratching condition (*i.e.*, load and rate) that can cause certain scratch and mar damage using a simple scratch test. This problem, however, may be overcome if the test device is built with the capability to execute increasing load or rate tests over a scratch length. With that, one can readily resolve the critical load or rate over which an expected surface damage occurs. This will inevitably save laboratory time and labor to determine and compare the scratch resistance for a given set of polymers.

CHAPTER III

EVALUATION AND QUANTIFICATION OF SCRATCH

3.1 Introduction

The great attention paid on aesthetics of polymer surfaces in recent years has led to significant interests in the scratch resistance and visibility of polymers. To this end, reliable methods to quantify scratch resistance and visibility become the top priority. The methods used in the quantification of scratch properties are mainly grouped under two categories depending on the parameter that is being measured. They are the measurement of physical dimensions, *i.e.*, scratch depth and width, and surface reflectivity. This chapter will focus on discussing the methods available to achieve the above measurements. Current developments on quantification of surface damage and scratch evaluation will also be addressed.

3.2 The Surface Phenomena of Scratch

A paper titled “The hardness of poly(methylmethacrylate)” (PMMA) published by Briscoe et al. [9] in 1996 proposed the basic theoretical background in analyzing scratch on polymers. Using the work done on metals by Bowden and Tabor [50], Briscoe et al. investigated the scratch properties of PMMA. Conical steel indenters of semi-angle ranging from 60° to 150° and at different loads were used to perform scratch on PMMA. The paper presented a scratch map of PMMA, whereby the different damage mechanisms were delineated in the map. The following mechanisms were

recognized: 1) ductile ploughing, 2) viscoelastic-plastic ploughing, 3) brittle cracking, 4) brittle deformation and 5) machining.

The ploughing process is also sensitive to many other factors, such as rate and temperature that further complicate the effort to predict such phenomena. Cutting and fragmentation are modes of material removal. Cutting produces ribbons of material in front of the scratching tip and is associated with ductile failure; whereas machining or fragmentation¹ produces fragmented debris from the substrate and is associated with brittle failure [51].

By measuring scratch hardness and indentation hardness, the authors were able to discern a linear relationship when conical angle is high. The effect of lubrication was also investigated and was found that lubrication increased the scratch hardness but decreases the indentation hardness. The scratch map that was the result of this work is useful in predicting the type of damage that might occur under different conical angles and load.

Other attempts by researcher to classify the different scratch behaviors that polymers exhibit have resulted in the construction of different scratch maps [16,38]. The scratch maps allow prediction of scratch behavior of specific polymers at different conditions such as cone angle, normal load, scratch width and tip geometry. It should be worth noting that Bertrand-Lambotte et al. [38] used the fracture energy and sample size criteria to predict ductile/brittle transition in nanoscratch of automotive clear-coats. A scratch map was constructed based on this work seemed to explain scratch behavior reasonably well.

Researchers have also sought to analyze scratch by classifying the many different types of surface damage features observed. Ironing denotes the scratch behavior which results in smooth featureless grooves that are due to plastic or viscoelastic/viscoplastic deformation. When the scratching process moves into the ploughing regime, wave-like pattern [21], cracking [16], plastic drawing [52] and bamboo-like feature [53] are some of the damage features observed in experiments. The cause(s) for each type of damage

¹ Some authors use the term micromachining to describe machining at very small scale.

feature can be due to brittle or ductile mode of deformation, or both. Clearly, a wide range of surface damage phenomena can be observed during scratching of polymers, making it a major obstacle in fundamental understanding and prediction of scratch-induced damage in polymers.

At present, there is no definitive way to evaluate scratch resistance or surface damage of polymers. Analytical models for scratch has been developed that are based on concepts analogous to indentation hardness [54]. Quantities such as scratch and ploughing hardnesses have been used to characterize the scratch resistance of metals. Briscoe and his colleagues [31] redefined the ploughing hardness as *tangential hardness* to include the adhesive contribution and specified another new hardness parameter called *dynamic hardness* for the purpose of their study or some authors refer to it as specific grooving energy [33]. To understand the terms given above, a list of definitions is given below in Table 3.1:

Table 3.1 :List of definitions of hardness

Term	Definition	Units
Indentation Hardness [54]	Normal load over projected load bearing area	MPa or Kgmm ⁻²
Scratch Hardness [54]	Normal load over projected load bearing area	MPa or Kgmm ⁻²
Ploughing Hardness [54] or Tangential Hardness [31]	Tangential force over projected area	MPa or Kgmm ⁻²
Dynamic Hardness [31] or Specific Grooving Energy [33]	Energy loss per unit deformed volume	N mm ⁻²

Thus, determining the scratch depth or width of a scratch groove will enable one to obtain the desired hardness value by calculating the relevant contact area. This provides an important tool for quantifying the scratch resistance of a polymer. Scanning electron microscopes (SEM) and optical microscopes are the common instruments used in inspecting the scratch surface of a material. This allows minute deformation mechanism(s) to be observed. Scratch widths can be measured using these methods. Scratch width measurement is by far the most popular method because of its ease of observation. On the other hand, precise depth measurements are not possible.

To overcome this, 3D laser profilometry and laser scanning confocal microscopy (LSCM) allow the 3D imaging of the sample surface. A huge advantage is gained by being able to analyze damage feature in 3-D. Not only can we make physical measurements (such as depth and heights), any pattern that can be observed using conventional SEM and optical microscopes can also be observed using this method. Atomic force microscopy (AFM) and scanning probe microscopy (SPM) are also used to obtain surface imaging. However, this method is limited to the nanometer and micrometer ranges.

3.3 The Visibility of Scratch

A scratched surface will reflect light in a different manner from an unscratched surface. By measuring the difference in the average intensity of the light reflected (reflectivity), scratch damage and visibility can be quantified [55].

Kody and Martin [28] used polarized light on a reflective optical microscope (Nikon Optiphot) to measure the reflectivity of surfaces. A Sony DXC-101 video camera was used to capture the reflected light after it has passed through the polarizer. The signal from the camera was digitized using a Scion Video Image 1000 8-bit frame grabber board and analyzed with NIH Image version 1.37 software. Figure 3.1 shows the basic principle of this method. The intensity of the reflected light was measured

when the scratch direction is parallel to the incident polarized light (where $\beta = 0^\circ$) and when it is at 45° (where $\beta = 45^\circ$). The two quantities were named B and D, respectively. Using the following definitions

$$\begin{aligned} S_a &= (B + D)/2 \\ S_d &= (B - D) \end{aligned} \quad (3.1)$$

It is possible to correlate S_a to the void formation during deformation and S_d to anisotropy caused by polymer chain alignment. Thus, visibility of the scratch and the contribution due to stress whitening was quantified by measuring the reflectivity.

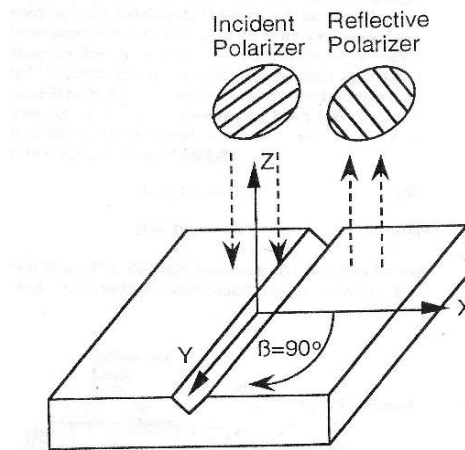


Figure 3.1: Schematic of light-scattering measuring apparatus (Kody et al. [28]).

A recent paper by Rangarajan et al. [56] describes using bidirectional reflectance distribution function (BRDF) experiments in quantifying scratch visibility. The experiments involve a laser light source to bounce off a specimen surface at -30° to the normal. A black and white charge coupled device (CCD) is placed $+30^\circ$ to the normal above the scratch surface to collect the specular reflected light. Another CCD is placed

at -10° to measure off-specular scattering. The former measurement gives information on the scratch size and surface specular reflectance. The latter measurement gives information on color and gloss of the scratch.

A third method used by Wang et al. [20] measured the light intensity reflected off a scratched surface using an optical flatbed scanner (ASTRA 1200S), then processed the information by digitizing the data using Scion Image 2 software and plotted a gray level profile across the scratches. The imaging software would assign values from 0 to 255 for each level of intensity. A profile plot over the scratch can be obtained. This method can be applied over a certain point on the scratch or over the whole length. It was found that scratch visibility was largely due to stress-whitening, and increases with normal load and addition of talc. This is a convenient way of comparing the scratch visibility level, and it can be done simultaneously over many scratches. Different variations of this method were also used by Chu et al [24-26] and Grasmeyer [27] to obtain gray level plots.

3.3.1 VIEEW[®]

Light that is reflected off a surface can be separated into two components, namely, diffuse and specular reflections. The diffuse component is responsible for the perception of color. Thus, any changes in color due to scratching can be measured by detecting the changes in diffuse reflection. The specular component is responsible for gloss of a surface. Any changes in surface roughness and topography will affect gloss. A commercial image analysis tool, VIEEW[®] (Atlas Material Testing Technology) [57] has the capability to produce ideal diffuse light condition *via* red, green and blue light-emitting diodes (LED). The amount of color in the diffuse light can be precisely controlled by changing the intensity of the LEDs. This is useful in characterizing any

stress-whitening that occurs. VIEEW[®] can also produce a beam of white light projecting 90° onto the surface. By measuring the light that is directly reflected back, the machine is able to detect edges of the scratch groove, thereby providing an accurate measure of scratch width. This analytical tool will be employed in the present study concerning scratch visibility.

3.4 Issues Concerning Evaluation and Quantification of Scratch

Polymers present a unique case in scratch. Unlike metals and ceramics, viscoelastic effects allow polymers to recover quickly after scratch. Scratching of polymer surfaces can often produce different surface features concurrently or sequentially [21,53]. Fillers and additives can add to the complexity of the surface damage features observed, where stress-whitening often occur due to the formation of voids and exposure of filler particles [20,58,59].

Polymers undergo ironing, ploughing, cutting and fragmentation like metals do. Determination of types of damages occur during scratch is of great concern to tribologists. Ability to identify a criterion or a set of criteria to predict the type of damage feature during a scratch process is of paramount importance to polymer scientists today. This knowledge has implications in applications where polymers are used as structural or coating materials. Introducing scratches on the surface can result in a drop in fracture toughness of the polymer. In coating materials, delamination will occur if the scratch extends too deep into the coating layer. The severity of the scratch is dependent on the type of scratch damage that occurs, thus the ability to predict scratch behavior will allow polymer scientists to greatly extend the utilization of polymers for new engineering and value-added applications.

An additional problem in the study of scratch on polymers is the multitude of test methods employed. Differences in test conditions and methodology will produce very different scratch behavior and damage features. This concern has been raised by Wong et al. [52]. It has been proposed that the progressive load test be employed as a standardized scratch test, which allows for a better link to material parameters and for easier comparison of results. The present work will thus follow the newly proposed test method to study the scratch behavior of polymers.

Another major concern to polymer scientists and engineers is the visibility of scratches on polymer surfaces. Polymers in automotive interior and exterior parts are susceptible to marks and scratches that vastly degrade their appearances. Polymers that exhibit high scratch resistance are highly desirable. Visibility is a complex issue as it involves many different unquantifiable parameters that can affect how a viewer perceives a scratch. Many attempts have been made to quantify scratch visibility by measuring the surface reflectivity of the scratch [20,27,28,55,60]. Due to the diverse techniques employed and the lack of a systematic study to correlate scratch features with visibility [61], the results obtained for one set of study is often valid only within a set of narrowly defined conditions [55]. It remains to be seen which of these methods, if any, will prove to be the most useful in characterizing scratch visibility.

3.5 Summary

A comparison of the different evaluation techniques discussed is given in Table 3.2. The merits and disadvantages of each method are also briefly discussed. In summary, scratch hardness is the most relevant technique in quantifying scratch resistance because it can be measured easily and applied to any material. Various techniques can be employed to acquire force and scratch width and depth data to obtain scratch hardness. Scratch visibility is a much more complicated issue, as there is no

simple relationship to link reflectance of a surface to human perception of a scratch groove. For PP, it has been shown that stress-whitening is the major contributing factor to scratch visibility, thus VIEEW[®], which is especially useful in quantifying stress-whitening, will be used in this work.

Table 3.2: Comparison of various techniques used in evaluation of scratch.

Technique	What it can be used for	Advantages	Disadvantages
Light /laser Interferometry	Measuring scratch depth and width, cross-section profile	Fast, noncontact scanning,	2D scanning
Stylus Profilometry	Measuring scratch depth and width, cross-section profile	Fast	2D scanning, deforms specimen, low res.
Digital Image Analysis	Gray level profile, stress-whitening	Fast, low cost	Relative values only
Optical Microscopy	Scratch surface features, scratch width	Fast, low cost	Surface scanning, low magnification, Subjective
Scanning Electron Microscopy (SEM)	Scratch surface features, scratch width	High magnification	Surface scanning, Subjective
3D Laser profilometry	Scratch depth and width, reflectivity, 3D imaging	3D scanning, noncontact scanning, high resolution	High cost
LSCM	Scratch depth and width, reflectivity, 3D imaging, subsurface imaging	3D scanning, noncontact scanning, high resolution	High cost
AFM	Scratch depth and width, 3D imaging	3D scanning, nanoscale resolution	High cost, slow
VIEEW[®]	Stress-whitening, scratch width	Easy operation, fast	High cost

CHAPTER IV

A NEW SCRATCH TEST METHODOLOGY FOR POLYMERS

4.1 Introduction

A new scratch test methodology is developed here. Different test conditions are used in conducting the scratch tests. The results is compared and assessed to determine the best method. Results from a concurrent study using finite element analysis (FEA) will also be presented.

4.2 Experimental

4.2.1 Custom-Built Scratch Test Device

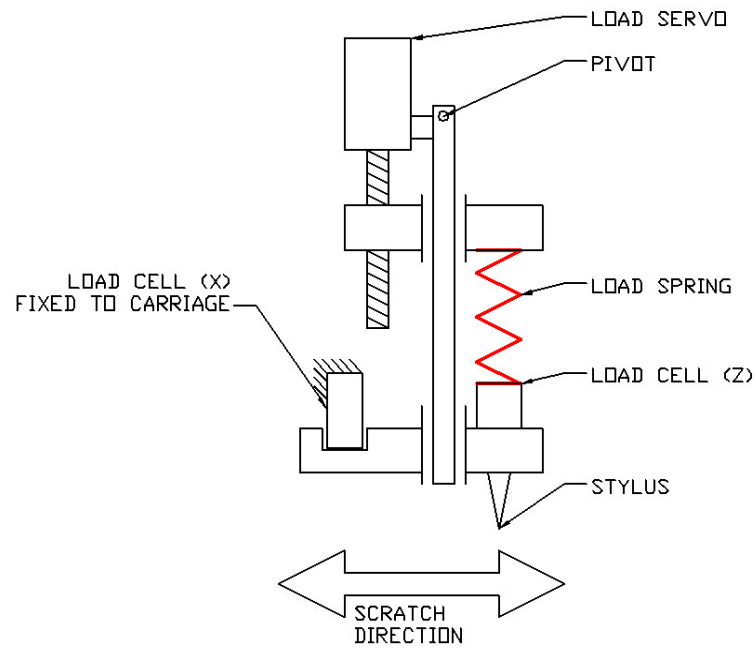
A new scratch device was developed for this research [62]. Though the focus of the research is mainly on automotive applications, the custom-built scratch device shown in Figure 4.1 is designed with various functionalities to address macroscopic scratch issues for a wide range of applications. These various functionalities are discussed below.

The scratch test device is built with the capability to execute multi-pass, multi-indenter, constant load, constant rate, increasing load and increasing rate tests under various operating temperatures. The scratch test unit comprises of a servo gear-driven motor that drives the scratch tips or styli with constant or linearly increased rates. For

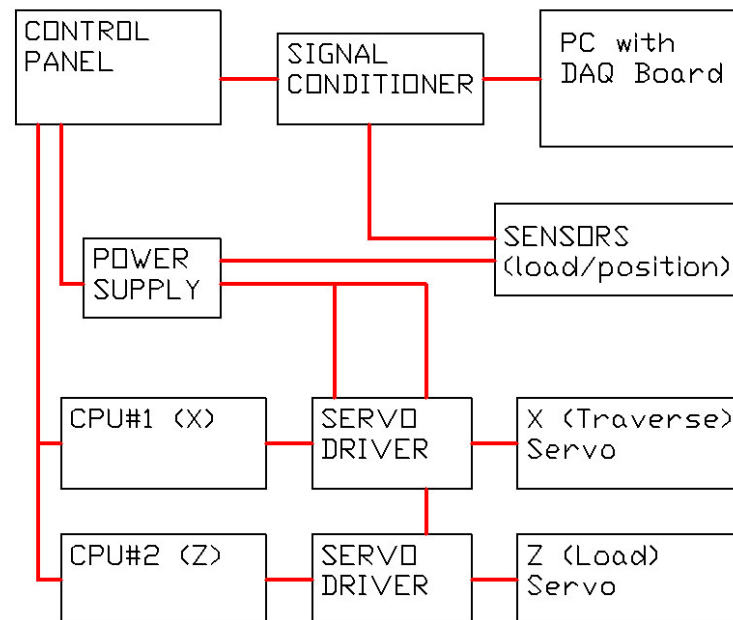
constant rates, the stylus can move in a range from 0 to 400 mm/s. As for linearly increased rates, the stylus can be set to move from a zero rate to a peak rate of 400 mm/s. A choice of up to five scratching styli can be used for the scratch test device to perform single- or multi-pass tests. The test device is also designed to conduct tests with dead weights or load-controlled spring loads. This allows the test device to have a wider load range for testing: 0 – 50 N for dead weights and 0 – 100 N for spring loads with a load control accuracy of 0.01 N. The reasons for incorporating spring loads are not only to allow for operation of increasing-load tests but also to prevent the occurrence of chattering of indenters as found in the dead weights loading case [63].

The test device is also equipped with sensing and data acquisition functions to record vital test data during testing, such as the tangential force acting on the stylus with an accuracy of 0.1 N for a load range up to 1,000 N. The data acquired for depth, horizontal position and velocity of the stylus have accuracies of 0.5 μm , 0.5 μm and 10 $\mu\text{m/s}$, respectively. During tests, these test data will be fed to an external computer for data storage and processing. Test parameters, such as number of scratch passes, start and end positions and rates of the stylus, are controlled through an on-board microprocessor housed in an instrumentation unit. An environmental chamber has been incorporated into the design of the test device (not shown in Figure 4.1) to allow scratch tests to be conducted under specified temperatures (-50°C to 100°C). Table 4.1 shows the comparison of the functionalities between our test device and the selected devices in the literature [15-21, 23, 30]. It is clear that the new machine compares favorably to the other existing devices. More importantly, researchers can use the new scratch test device to design a variety of scratch tests on different polymeric bulk or coating systems through its various intended functionalities; some of these suggested tests are shown in Table 4.2.

Several of the suggested tests are applied to the model polypropylene (PP) systems to illustrate their usefulness in scratch characterization. In the description of the scratch tests, emphasis will be placed on the test procedure and scratch damage quantification to help establish a standard test method for scratch evaluation of polymers.



(a) Schematic of the spring-loaded scratch tip.



(b) Schematic of control system of scratch unit and data acquisition unit

Figure 4.1: Design of the custom-built scratch test device.

Table 4.1: Comparison of functionalities of different scratch devices.

Functionality	Scratching machine by Briscoe et al. [15-18]	Scratch Apparatus by Gauthier & Schirrer [19]	Scratch test rig by Wang et al. [20]	In-house scratch test apparatus by Ni & Faou [21]	Revetest Scratch Tester [23]	Scratch Resistance Tester [30]	Current Custom-Built Scratch Device
Constant Load Test (Range)	Yes – dead weights	Yes (0.05 – 5N)	Yes (1 – 100N)	Yes (0.1 – 10N)	Yes (1 – 200N)	Yes (0–0.59N)	Yes (0 – 50N : dead weight) (5 – 100N : spring load)
Constant Rate Test (Range)	Yes (0.001 – 40mm/s)	Yes (0.01 – 100mm/s)	Yes (1 – 200mm/s)	Yes (0.011 – 0.46mm/s)	Yes (0.003 – 6.67mm/s)	Yes (8.33–166.67 mm/s)	Yes (0 – 400mm/s)
Increasing Load Test (Range)	No	No	Yes (1 – 100N)	No	Yes (0.01 – 30N)	Yes (0–0.59N)	Yes (5 – 100N)
Increasing Rate Test (Range)	No	Yes (0.01 - 100mm/s)	No	No	No	Yes (8.33–166.67 mm/s)	Yes (0 – 400mm/s)
Temperature Control (Range)	Yes	Yes (-70 to 120°C)	Yes	No	No	No	Yes (-50 to 100°C)
Multi-Indenter Test	No	No	No	No	No	No	Yes
Data Acquisition	Yes	Yes	Yes	Yes	Yes	No	Yes
Optical Observation Device	No	No	No	No	Yes	No	No (provision provided for upgrading)

Table 4.2: Suggested tests for scratch characterization.

Important Scratch Characterization	Suggested tests
Effect of scratch rate	Increasing rate tests
Effect of scratch load	Increasing load tests
Effect of temperatures	Scratch tests with environmental chamber
Influence of multiple scratches	Multiple-indenter tests

Table 4.3: Composition of PP systems.

Material System	PP type	Filler (wt. %)	Coloring Compound (wt. %)
1	Homopolymer	—	2NCA (2%)
2	Homopolymer	Talc (20%)	2NCA (2%)
3	Copolymer	—	2NCA (2%)
4	Copolymer	Talc (20%)	2NCA (2%)

4.2.2. Model Material System and Test Procedures

In this study, four PP-based material systems are selected and their compositions are shown in Table 4.3. For these material systems, the PP resin and a dark gray coloring pigment was provided and blended by Solvay Engineered Polymers. Talc additive was provided by Luzenac. Injection molding of the plaques, having dimensions of 340 mm × 180 mm × 3 mm, was performed by Advanced Composites, Inc. For testing, the plaques were cut and

machined into dimensions of 140 mm × 1 mm × 3 mm. All test specimens were prepared according to ASTM D 618-00 Procedure A [64].

Three sets of scratch tests (Tests *A* – *C*) were conducted. In Test *A*, a constant stylus rate of 100 mm/s with a linear increasing normal load of 0 to 50 N was performed. While in Test *B*, a 30 N dead load was utilized with a constant stylus rate of 100 mm/s, which is consistent with the Ford *five-finger* test. Finally for Test *C*, a dead weight of 30 N was used with a linearly accelerated stylus rate of 0 to 140 mm/s. The scratch lengths of all tests were set to be 100 mm and tests were conducted at room temperature. Stainless steel ball with a diameter of 1 mm was used as the scratch stylus tip.

4.2.3. Evaluation of Scratch Damage

Transmission optical microscopy (TOM) observation, using an Olympus[®] BX60 microscope, of thin sections of PP systems was performed to study the scratch damage of selected cross-sections along and across the scratch groove. The thin sections were prepared by cutting the polymer strips into 2-cm long rectangular blocks, and mounted in an epoxy resin. The mounted polymer block was glued onto a microslide and further cut down to a 2-mm thick section by an ISOMET[®] 1000 diamond saw. The thick sections were then polished to a thickness of 100–150 μm , using polishing papers stepwise with roughness from grit 800 to grit 4000 (grain size 5 μm) to achieve the final polish.

Scanning electron microscopy (SEM) was also performed to study the microscale surface damage features using a JEOL JSM-6400 system. A flatbed scanner with a resolution of 1,200 dpi was used to scan the test specimens and generate digital images for the quantification of scratch damage.

To quantify the scratch damage, measurements were taken from the TOM, SEM and scanned images using the definitions of scratch widths and depths by Kotaki et al. [65], as shown in Figure 4.2. *SW1* represents the inner

width of the scratch groove. $SW2$ represents the outer width of the scratch groove, *i.e.*, the distance between the points where the slopes of the hills meet the unscratched plane. $SD1$ represents the depth of the scratch groove calculated from the unscratched plane. $SD2$ is the height of the peak to the trough of the scratch groove. For spherical indenters, the scratch grooves generally show a symmetric cross-sectional profile. In cases where asymmetry occurs, *i.e.*, one side of the pile-up is higher than the other; the higher point was taken to obtain scratch depths.

4.3. Finite Element Analysis

In the concurrent work by Goy Teck Lim [52], in the mechanics of scratch, the finite element method [66] is used as the numerical tool to help elucidate the phenomena observed in the experiments. A well-established commercial package ABAQUS/Explicit® [67] has been adopted to perform the finite element analysis (FEA) of the concerned problem.

The modeling work is primarily set out to model the scratch problem as closely and realistically as possible to the actual testing conditions. A computational model of 50 mm × 10 mm × 3 mm was first considered. By exploiting the plane of symmetry, the computational model was reduced to the dimensions of 50 mm × 5 mm × 3 mm, as illustrated in Figure 4.3. Not only will it save computational resources, the results of the reduced computational model can be extended to those of the original model. For a more detailed discussion of the boundary and loading conditions of the computational model and various considerations of the FEA, one can refer to the literature [52, 68, 69].

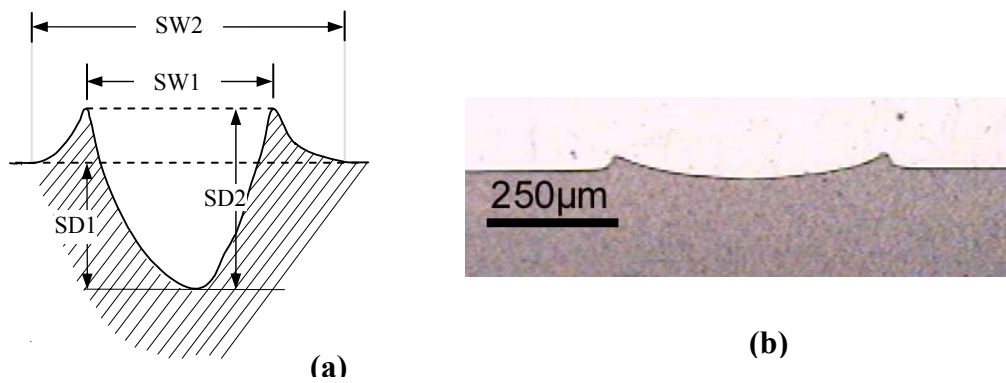


Figure 4.2: (a) Definitions of scratch widths and scratch depths; (b) Actual cross section of a scratch groove.

4.4. Results and Discussion

4.4.1. Experimental Results

The scratch damage cross-sectional profile is reported based on an average of five specimens for each test condition. For Test *A*, the cross-section was taken at a location equivalent to 30 N load. While for Test *C*, the cross section was taken at a location equivalent to 100 mm/s speed. In this way, the three tests could be compared under the same loads and speeds of 30 N and 100 mm/s.

Following the definition specified in Figure 2, the trend suggests that the scratch width is the greatest for Test *C*, followed by Test *B* and Test *A* (Figure 4.3a). This trend has also been observed in FEA modeling (Figure 4.3b), which will be discussed in the next section. For Test *C*, the accelerating scratch tip will induce both horizontal (in the direction of scratch) and vertical inertias (acting downwards). The vertical inertia induced is due to the frictional effect. Both of the inertia will increase the normal and tangential forces acting on the substrate, thereby increasing the scratch width and depth. While the increasing load imposed in Test *A* also induced additional vertical inertia, the magnitude of

the induced inertia is much smaller than that for Test *C*. With the presence of induced inertia, it is however contrary to the engineering intuition that the scratch width for Test *A* is smaller than that for Test *B*, where there should not be any additional inertia induced. One possible reason for such an anomaly is because of the pre-existing high penetration depth due to the high initial dead load for Test *B*, which leads to a much higher resistance against horizontal sliding. This, in turn, induces a higher ‘scratching force’ required to drive the scratch tip to maintain a constant speed of 100 mm/s, when compared to Test *A*.

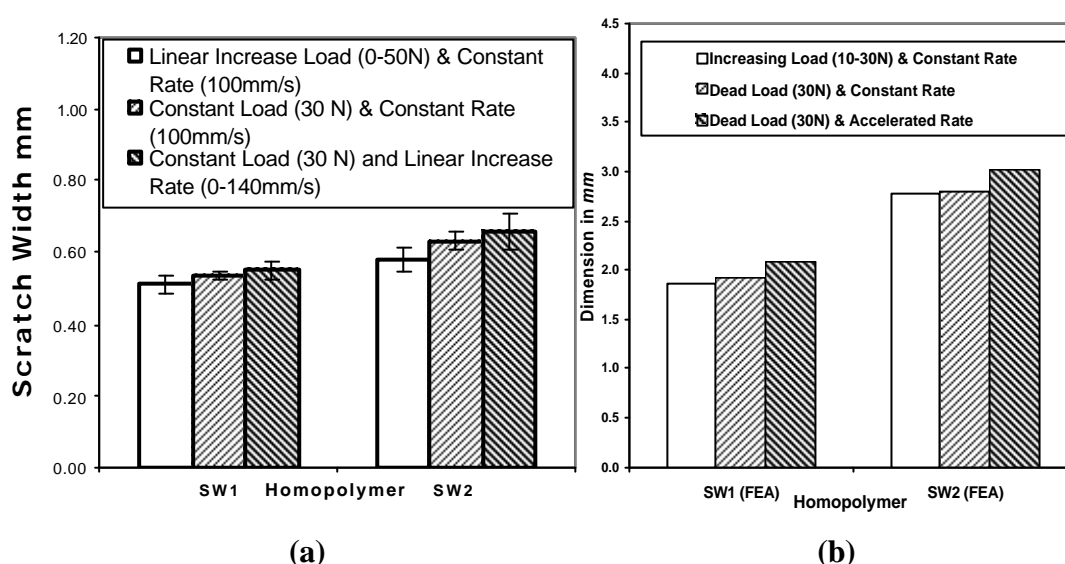


Figure 4.3: Comparison of (a) experimental and (b) FEA results.

Comparing the scanned images of the scratch morphology of a talc-filled PP copolymer under the three test conditions, the scratch width remains constant along the scratch path for Test *B* and *C* conditions; while there is a gradual increase in scratch width along the scratch path for Test *A* (Figure 4.4). The damage induced in the scratch groove undergoes a transition as the scratch progresses in Test *A*. Minimal surface features are observed in the beginning while severe damage with prominent ripple marks is present toward the end of the scratch. It is found that the ripple marks are actually curved fracture lines

that appear periodically. The same phenomena are also observed in other model PP systems. It should be noted that the existing initial scratch width of 0.33 ~ 0.45 mm found in specimens is caused by the pre-existing small mass of the scratch tip and the load control unit, which measures about 5 N. Future improvement to the test device will be made to minimize such a pre-existing dead load prior to testing.

It is apparent that the linear load increase test, *i.e.*, Test A, is a more sensible test method in characterizing scratch damage resistance in polymers. Subsequent tests done on different material systems will demonstrate the usefulness and effectiveness of this test. The test has shown that copolymer systems suffer more damage than homopolymer systems (Figure 4.5). This is to be expected as the Young's modulus and yield strength of copolymer PP are lower than those of the homopolymer PP [70]. Interestingly, the addition of talc does not cause significant changes in the size of scratch damage as quantified by the scratch depths and scratch widths. The test also found that all scratch depths and scratch widths show the same general trend between the copolymer and homopolymer PP, and between neat and talc-filled PP systems.

Figures 4.6 and 4.7 illustrate a typical complex surface feature and its sub-surface damage profile after a scratch is performed on a polymer. It is evident that complex surface damage mechanisms, such as plastic ironing, brittle fracture, fibril drawing, filler debonding, stick-slip, etc., can evolve, causing the scratch depths to vary within the same scratch pass. Thus, it is recommended that scratch widths, as opposed to scratch depths, be considered as a more reliable and consistent measure to quantify scratch damage. Adopting the scratch widths as a measure of severity of surface damage can be quite practical since flatbed scanners can be used for the measurement. However, it should be highlighted that the scanned images generally have a relatively lower resolution than TOM or SEM images. Hence, one cannot easily distinguish between SW1 and SW2 from the scratch widths measured from scanned images. Nevertheless, scanned images allow one to have a quick assessment of the scratch damage. More sophisticated imaging tools can always be used for a more detailed study, if needed.

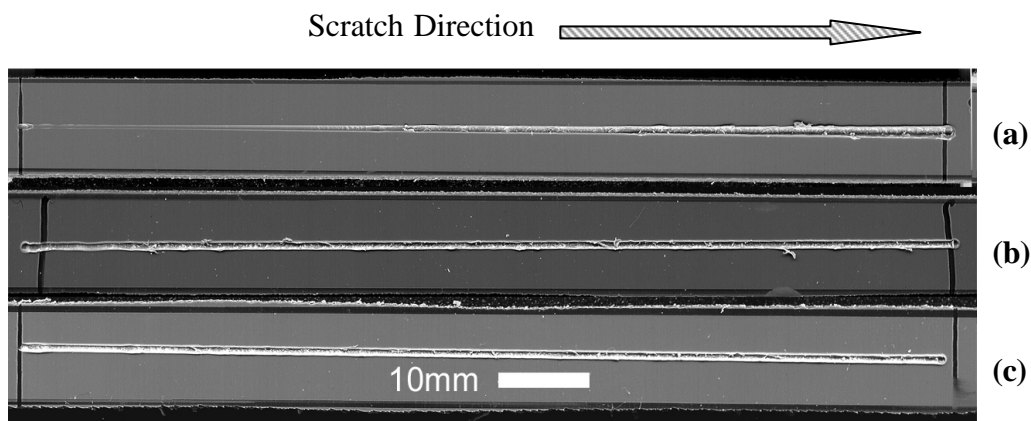


Figure 4.4 : Talc-filled copolymers scratched under different conditions. (a) Linear load increase and constant speed, (b) constant speed and load and (c) linear rate increase and constant load.

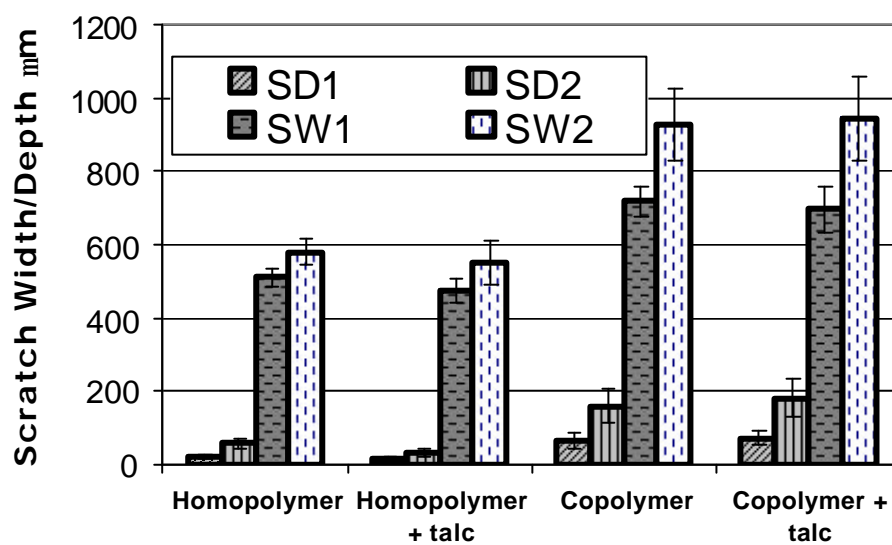


Figure 4.5 : Scratch widths and depths from linear load increase test condition on four different model PP systems.

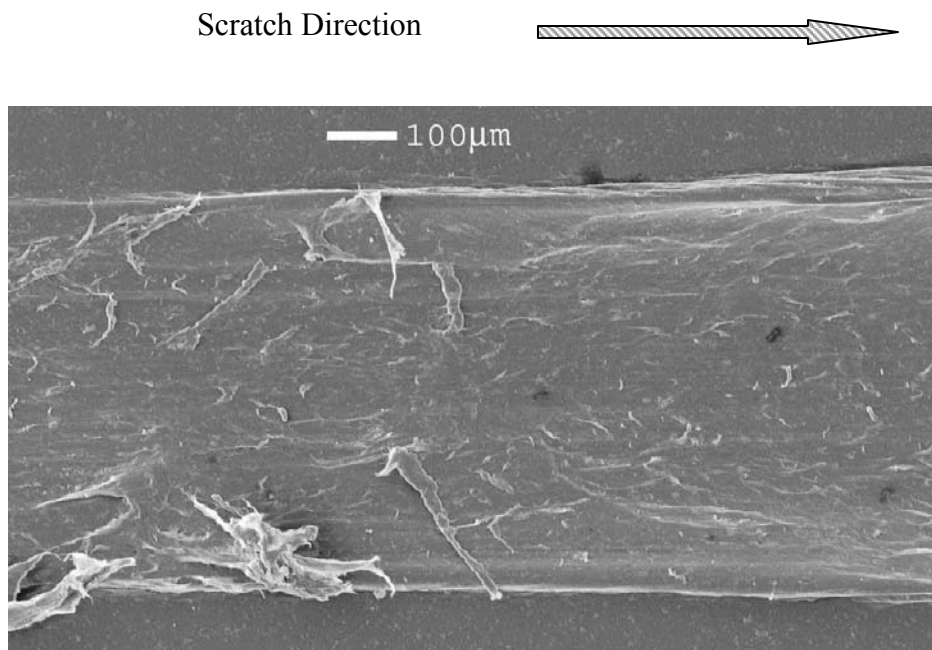


Figure 4.6: SEM of talc-filled homopolymer scratched under Test A conditions.

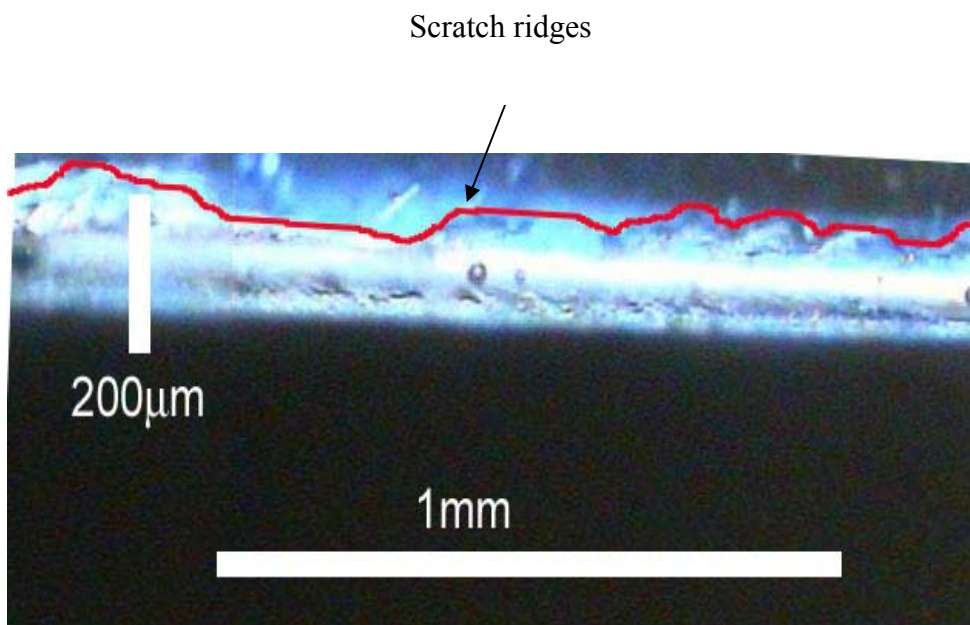


Figure 4.7: Variation of scratch depth along scratch groove in talc-filled copolymer.

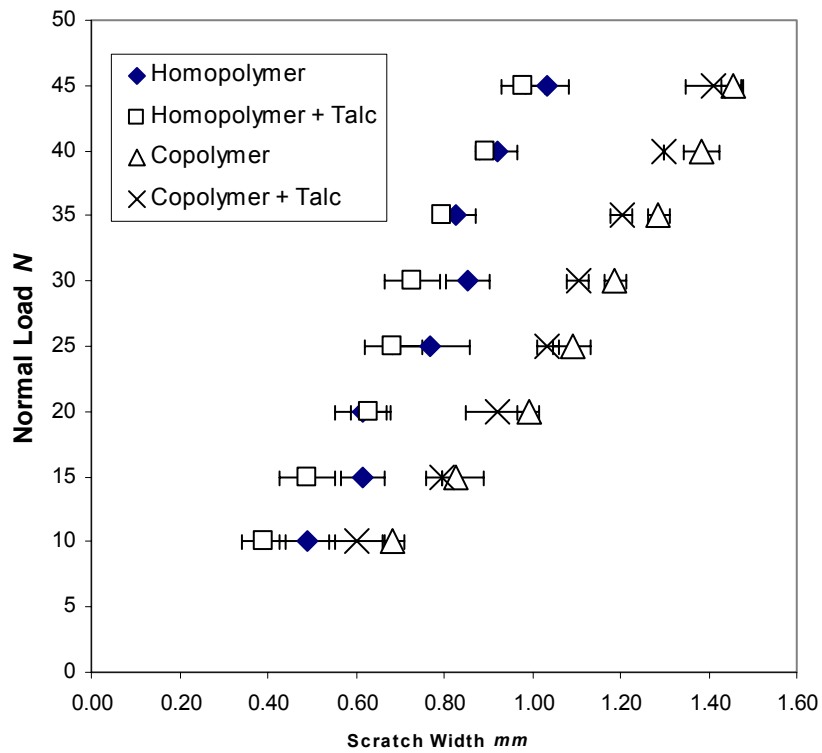


Figure 4.8: Variation of scratch width with normal load.

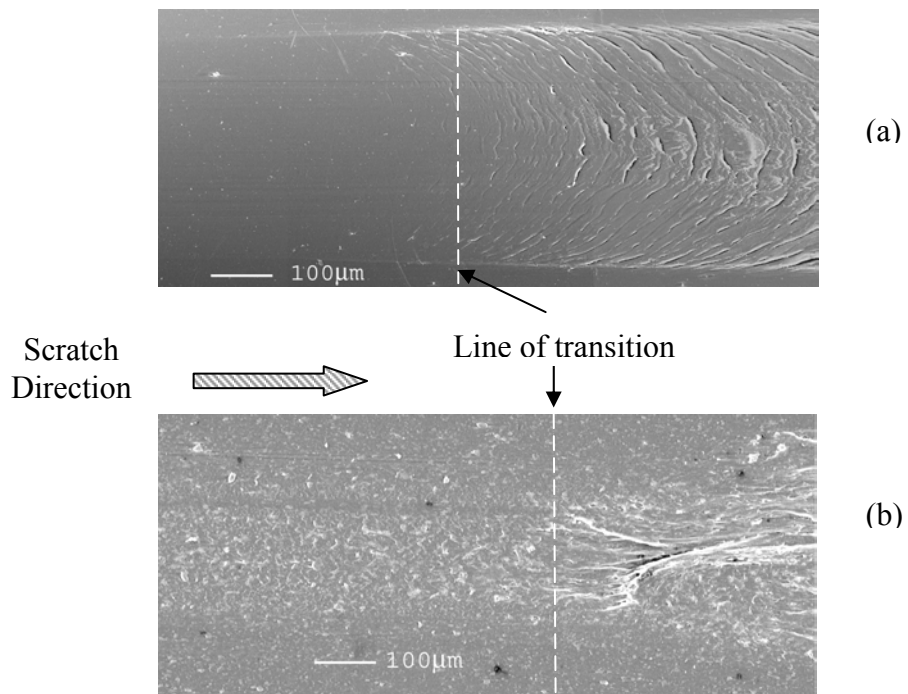


Figure 4.9: Mar-scratch damage transition of (a) homopolymer and (b) talc-filled homopolymer in Test A

To establish a relationship between scratch widths and normal loads, the linear load increase test as in Test *A* can be used. Figure 4.8 shows a plot of the nominal normal loads applied by the spring load against the scratch widths measured by the scanner for various PP systems. For all PP systems, the scratch width follows a reasonable linear relationship with normal load, with the copolymer PP exhibiting larger scratch widths than homopolymer PP. Figure 4.8 is a useful plot for revealing the load needed to form a given scratch width for a given polymer. Since it has been shown that scratch width correlates well with scratch visibility as well as the severity of surface damage if the surface damage characteristics stay the same [25], it is therefore possible to easily determine the critical load needed to cause such a surface damage based on the scratch widths data shown in Fig. 4.8. Most significantly, this plot will also allow material designers to quantitatively formulate a workable system to achieve specified surface damage resistance for a given polymeric system under a given testing condition.

Furthermore, the Test *A* method permits a mar-scratch transition to be identified. This will help determine the critical normal load for such a transition. For illustration, scratched specimens from Test *A* were scrutinized for the exact load and location along the scratch path where the scratch groove becomes highly visible. SEM images that show the mar-scratch transition for homopolymer and talc-filled homopolymer are given in Figure 4.9. The distance and normal load for the mar-scratch transition are also listed in Table 4.4. The damage modes for homopolymer and talc-filled homopolymer are observed to be distinctly different. For homopolymer PP, the surface is smooth with no prominent features except for the faintly discernable edges before the line of transition (see Figure 4.9a). After the line of transition, curved fracture lines appear and are closely spaced together, indicating an increase in the severity of surface damage. In addition, a change in damage mode from plastic ironing to plastic drawing and cracking is found as the load increases. For talc-filled homopolymer PP, before the line of transition, the surface damage is barely observable where a very shallow depression is formed due to the sliding of the scratch tip (Figure 4.9b). The scratch groove is so shallow that it is more

Table 4.4: Mar-scratch transition values.

	Homopolymer	Homopolymer + Talc
Mar-Scratch Transition Distance (cm)	2.65	1.90
Mar-Scratch Transition Load (N)	18	15

consistent with mar damage. After the line of transition, surface drawing and large-scale plastic deformation occur, creating the damage features that scatter light more significantly from the scratch groove.

The two SEM micrographs contrast the differences in surface damage mechanisms that occur during the mar-scratch transition. Homopolymer PP exhibits a more brittle damage mode, which is evidenced by the regular plastic drawing and crack lines; whereas talc-filled homopolymer shows more plastic drawing. This finding suggests that the addition of talc will alter the mode of scratch damage. This study also indicates that the addition of talc into PP will lower the normal load required to cause mar-scratch transition by about 3 N (Table 4.4). It should be noted that the critical load for the stress-whitening transition, which does not necessarily coincide with mar-scratch transition described above, can also be determined using the linear load increase test. The findings have been demonstrated by using a commercial image analysis tool, VIEEW[®]. The details of the results and their significance will be discussed in a separate paper.

The scratches performed under Test *B* and Test *C* do not exhibit such a transition. This is mainly due to the pre-existing severe initial indentation caused by the 30 N dead weight (Figure 4.4). From the width measurements and the gray level analysis *via* a scanner, it can be shown that the scratch width does not vary significantly along the scratch grooves for Test *B* and Test *C*. In contrast, the linear load increase test (Test *A*) does not introduce such a severe initial indentation because of its minimal starting load. The transition in damage can thus be observed. A scanned image shown in Figure 4.10 clearly

illustrates the transitions as the scratch groove progresses. Both the mar-scratch and the stress-whitening transitions can be observed.

Another advantage of using the linear load increase test is the prevention of “chattering” of the scratch tip. In the work done by Kita et al. [63], it has been found that at constant speed and constant dead weight test, the scratch tip has a tendency of skipping or jumping during scratching, depending on the polymer type and the testing conditions applied. The same effect has also been observed in scratch tests done under similar conditions in our study. This effect probably comes about when the tip ploughs too deep. When ploughing resistance becomes higher than scratching force, skipping occurs as the tip can only continue the forward motion by climbing up vertically. The linear load increase test eliminates this effect because the scratch depth is shallower and the frictional force that entails will not overcome the scratching force.

Figure 4.11 shows the normal load of the scratch stylus as it traverses a neat PP specimen. Notice that the load plot is linear and well-behaved without any large spikes, proving that severe chattering did not occur during the linear load increase scratch test.

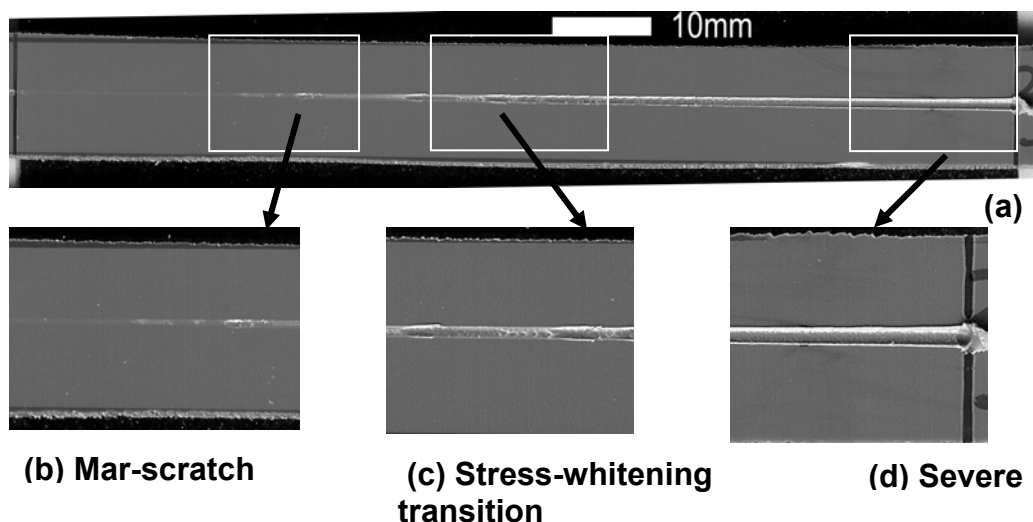


Figure 4.10: Scanned image showing scratch damage transition in a talc-filled homopolymer under Test A conditions. (a) Entire scratch length, (b), (c) and (d) are enlarged details showing transition in scratch damage.

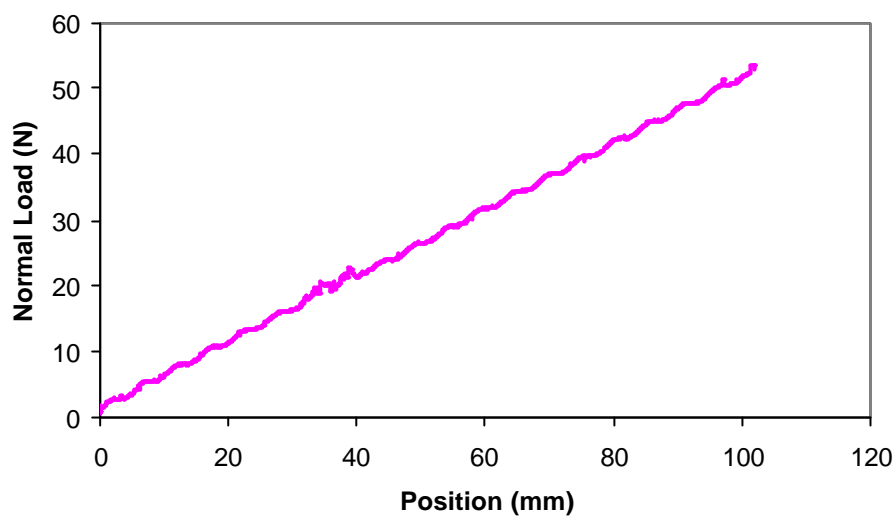


Figure 4.11 : Normal load profile of neat PP under linear load increase test during scratch.

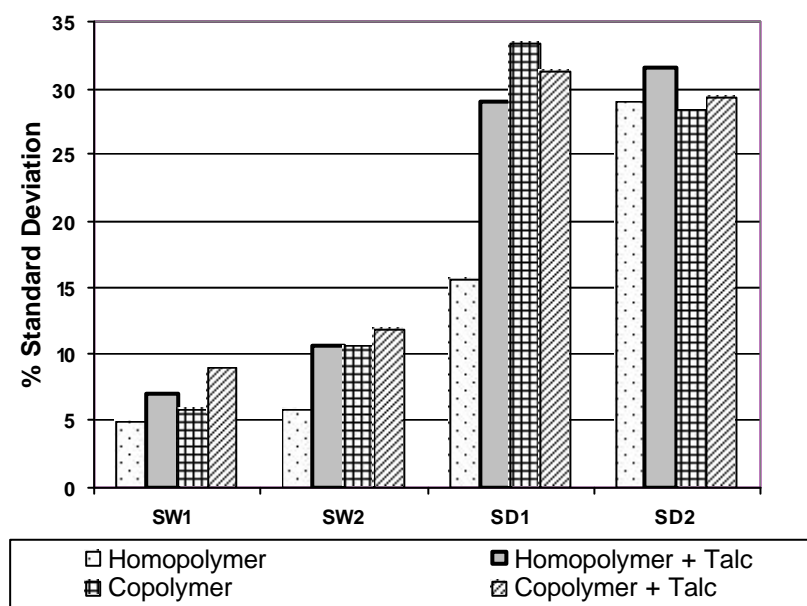


Figure 4.12 : Percentage standard deviation for scratch widths and depths in the linear load increase test.

4.4.2. Repeatability

The scratch tests performed above show that our custom-built scratching machine, if executed with care, can generate results that are highly repeatable. To show the repeatability of test results, standard deviation of the scratch widths and depths from Test *A* are calculated and plotted in Figure 4.12. From Figure 4.12, the percentage standard deviation is found to be lowest for SW1 and SW2, while it can go as high as 33% for SD1. This further suggests that the scratch widths give a more reliable measure of scratch damage. Apart from scanned images, the repeatability of test results in terms of scratch widths and depths has also been evaluated using a commercial image analysis system, VIEEW[®] and the findings are very similar to the analysis given above.

4.4.3. Numerical Analysis Findings

To evaluate the effect of loading conditions and scratch rates on the stress field of the computational model, three different load cases that are similar to the three tests performed in the experimental section (Tests *A* – *C*) were considered for the present FEA work. The three load cases¹ are: (*a*) linearly increasing load (10 – 30 N) under constant scratch rate, (*b*) dead load (30 N) under constant scratch rate, and (*c*) linearly increasing scratch rate under dead load (30 N). Using the same scratch damage quantification in Section 4.2.3, the scratch widths, SW1 and SW2 predicted by FEA at sections where the normal load and the scratch rate are the same for the three load cases, are shown in Figure 4.3. Good qualitative correlation can be noted.

¹ Note that the use of the reduced computational model in FEA (refer to [52]) requires the normal loads specified to be reduced by half [67]. The computed FEA results remain valid for the normal loads as stated.

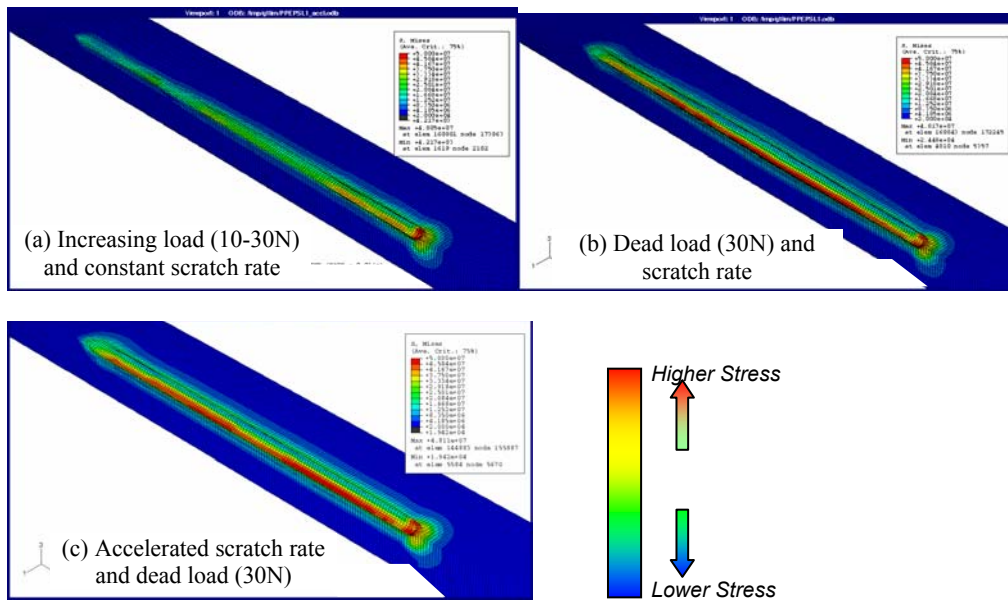


Figure 4.13: von Mises stress distribution for different load cases. (after Lim [52])

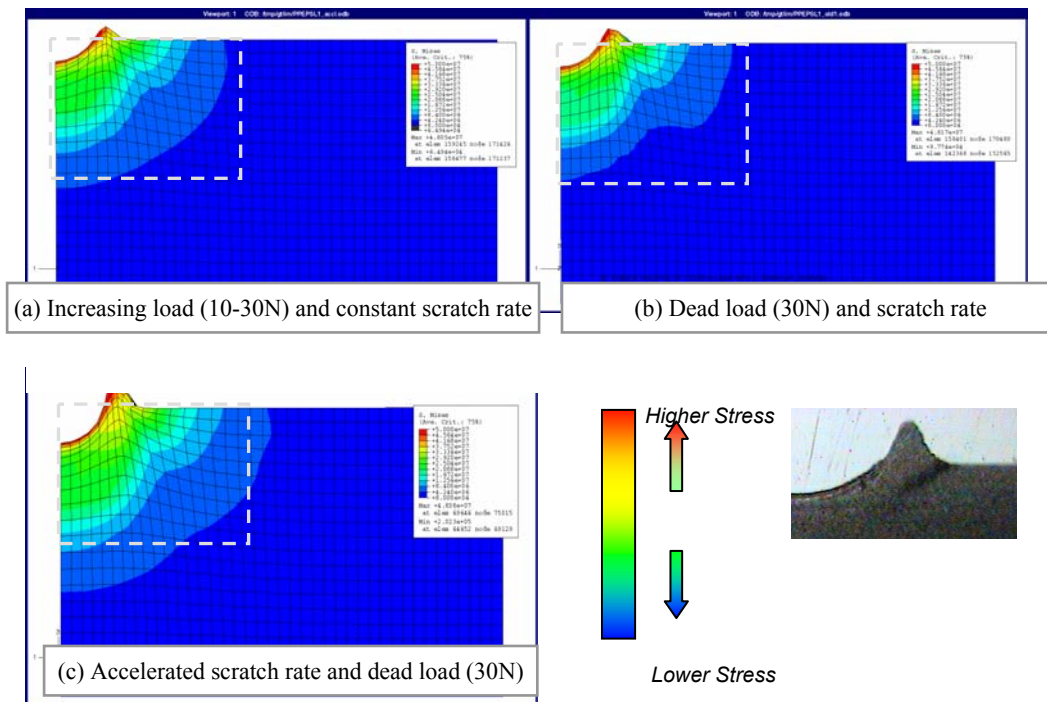


Figure 4.14: von Mises stress distribution for different load cases, cross – section view. (after Lim [52])

Similar to the earlier experimental findings, the scratch widths are found to be the smallest for load case (a), *i.e.*, Test *A*, followed by load case (b), *i.e.*, Test *B*, and load case (c), *i.e.*, Test *C*. There is, however, a noted quantitative difference between both sets of results and may be due to the material model adopted in the FEA, which may require further refinement.

The von Mises stress distribution of the computational model for the three test conditions are plotted in Figure 4.13(a-c). By contrasting the three contour plots, one can readily see that the computational model undergoes the least amount of plastic yielding for load case (a), followed by load case (b) and the most severe for load case (c). To have a more reasonable comparison of the von Mises stress distribution, the contour plots across the appropriate cross-sections where the normal load and the scratch rate will concur at the same value in all three load cases are presented in Figure 4.14. As shown in these figures, the change in the loading and scratch rates has a profound effect on the extent of von Mises stress distribution. To distinguish the differences in the loading effect, a viewing box is drawn over each stress zone, with the load case (b) taken as the reference. Through these viewing boxes, the increasing loading rate during scratch as in load case (a) will render the stress zone to extend slightly deeper into the substrate. By accelerating the scratch rate, as in load case (c), within the same scratch pass, the more critical stress zone not only deepens, but also widens. For a detailed explanation on the FEA results, refer to the papers by Lim et al. [52].

4.5. Conclusions

In the present work, a new scratch test method has been introduced to evaluate polymer scratch resistance. The proposed scratch test method is used to investigate four sets of model PP systems. By employing the linear load increase method, the chattering phenomena commonly seen in dead weight methods are eliminated, and the scratch damage resistance of different PP

systems can be quantified. It is found that copolymer PP suffers greater scratch damage than homopolymer PP. Addition of talc does not change scratch widths and depths of both homopolymer and copolymer significantly. Good repeatability in all three test conditions is also found using our custom-built scratcher. The proposed linear load increase test enables the observation of mar-scratch and stress-whitening transitions during scratch.

From the three-dimensional FEA, a better understanding of several influencing factors, such as the change in the loading and scratching rates and stress distribution around the indenter, is gained. Through the correlation between the FEA and experimental results, it is indicative that the FEA is able to qualitatively capture the important characteristics of the scratch process, and hence warrants further utilization of FEA for fundamental understanding of scratch behavior of polymers.

CHAPTER V

STUDY OF SURFACE DAMAGE OF POLYPROPYLENE UNDER PROGRESSIVE LOAD

5.1 Introduction

The main objective of the current work is to investigate the relationship between the surface damage features observed during scratch and the material parameters. It is intuitive that surface damage features and damage mechanisms transitions can be linked to the material characteristics and the stress state the material experiences. The frictional force exerted during scratching was recorded. Through the comparison of the frictional force profile and the damage features of the scratched surfaces, direct correlation among damage features, visibility and applied force can be achieved.

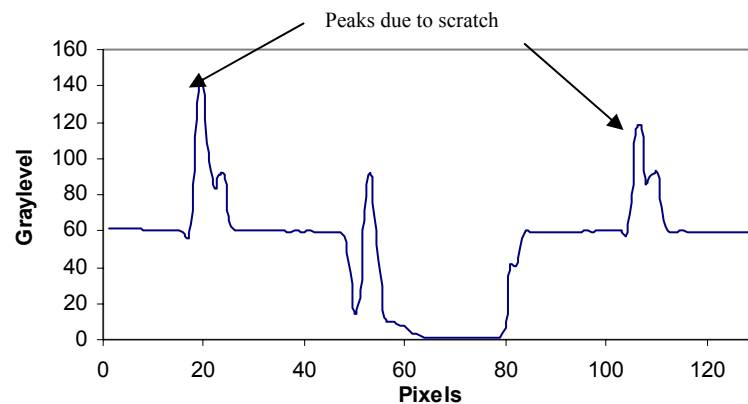


Figure 5.1: Gray level plot of scratch groove from scanner image.

5.2 Experimental

5.2.1 Experimental Approach and Materials

The experimental procedure and materials used are as described in Section 4.2.2. In this case, only specimens from the progressive load condition (Test *A*) were studied.

A second variation of the experimental procedure was introduced. Selected samples of the scratched specimens were immersed in water and sonicated for 30 min in a Branson[®] ultrasonic cleaner with an output power of 70 W at 42 KHz. The energy generated by the ultrasonic vibration is expected to preferentially remove remnant from the damage regions in the scratch groove that are highly stressed. The use of this technique will thus reveal regions where scratch induces the most damage.

5.2.2 Quantification of Scratch Damage

Scanning electron microscopy (SEM) was performed to study the microscale surface damage features using a JEOL JSM-6400 system. A flatbed scanner with a resolution of 1,200 dpi was used to scan the scratched surfaces to quantify scratch damage. A commercial image analysis tool, VIEEW[®], was also used to scan and quantify surface damage of the specimens.

Quantification of damage was performed in accordance to the earlier method described in Section 4.2.3. Thin sections were used in taking cross-polarized micrographs using the BX60 Olympus[®] microscope.

For scratch visibility evaluation *via* scanner, the scratched specimens were laid and scanned together with a piece of white Xerox paper. The scanned image was then

processed by adjusting brightness and contrast of the image so that the piece of white paper in the image has a value of 255 in grayscale. The gray level of the image is then measured using Scion Image Beta 4.0.2. The length of the scratch groove was divided into five equal sections, each with 2 cm in length. Figure 5.1 shows the gray level plot of two specimens that were scanned together. The values shown are the average gray level along the scratch groove within the 2 cm section. The peaks (indicated by arrows) show that higher amounts of light were reflected off the scratch groove than the surrounding areas.

In addition, VIEEW[®] was used to define areas that were stress-whitened during scratching. The onset of stress-whitening could thus be measured reliably. The corresponding critical distance and critical load can be obtained *via* this method.

5.3 Results and Discussion

5.3.1 Homopolymer Surface Features

Figures 5.2 and 5.3 show the scanned images of neat homopolymer and talc-filled homopolymer scratched under progressive loading. Various regions of interests are highlighted and SEM micrographs of these locations are also displayed in Figures 5.2(b)-(e) and 5.3(b)-(e). In Figure 5.2, Region 1 shows the characteristic wave-like deformation, which is seen in PP scratched under low loads and low speeds [24, 25, 70]. It has been shown by Tang and Martin [71] that these wave-like patterns are likely the result of shear bands formed near the surface of the scratch groove. Region 2 shows a transition in damage feature, the width of the groove increases more rapidly, the regular parabolic lines are no longer present and are replaced by irregular brittle type of failure. This suggests that shear banding is no longer the major mode of deformation. Fracture

lines are clearly visible, which are indicated by arrows in the micrograph. The scanned image also shows an increase in visibility because of the increase in whiteness of the groove. Interestingly, the damage pattern settles into a regular sigmoidal pattern after it has reached the maximum width (indicated by dashed line) and gradually fades away into a smoother groove. Region 3 shows another type of transition. In this case damage becomes more severe and the deformed material forms 'lips' that overflows to the side of the groove. This indicates an increase of pileup in the scratch groove. In the later stage of the scratch, surface damage is predominantly random fracture lines (indicated by arrows). Regions 4 and 5 shows that the damage features remain unchanged. Region 5 was subjected to sonication before SEM analysis. An anomaly that is attributed to the sonication process is observed in Region 5. More on this anomaly will be discussed in a later section.

Figure 5.3 shows a similar progression in severity of surface damage of a talc-filled homopolymer. However, there are some obvious differences. Firstly, a clear transition from mar to scratch is seen in Region 1. The surface damage is barely perceptible before transition except for a slight difference in surface texture from the unscratched surface. After the transition, a dramatic change in damage mode occurs with large plastic drawing. Region 2 shows a very similar type of transition as shown before in the homopolymer. Region 3 shows a rougher surface with debris (encircled in white), in contrast to the relatively smooth surface in Figure 5.2. It is observed that a segmented type of pattern appears in region 3, which suggests the occurrence of a stick-slip process. In region 4, the scratched surface shows a very rough texture with debris, fibrils and large pileups on the side. Thus, the evidence seems to suggest that the addition of talc affects the damage mode during scratch by inducing ductile deformation. Region 5 was subjected to sonication like in the previous example. Again, anomalous features were found that is attributed to the sonication process.

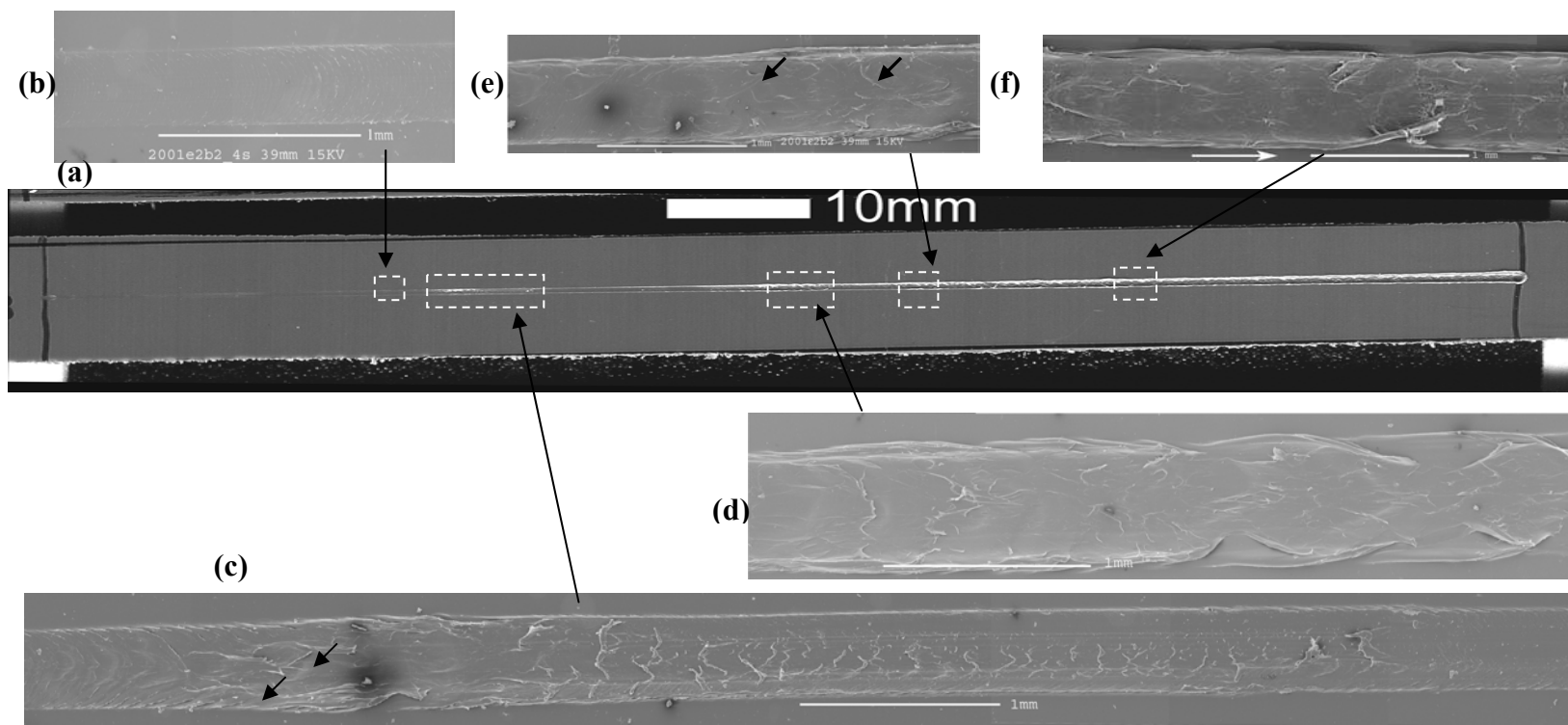


Figure 5.2: (a) Scanned image of scratched homopolymer, (b) region 1, (c) region 2, (d) region 3, (e) region 4 and (f) region 5 are SEM micrographs of highlighted regions in the scratch groove. Note that that region 5 shows fibril breakage after sonication.

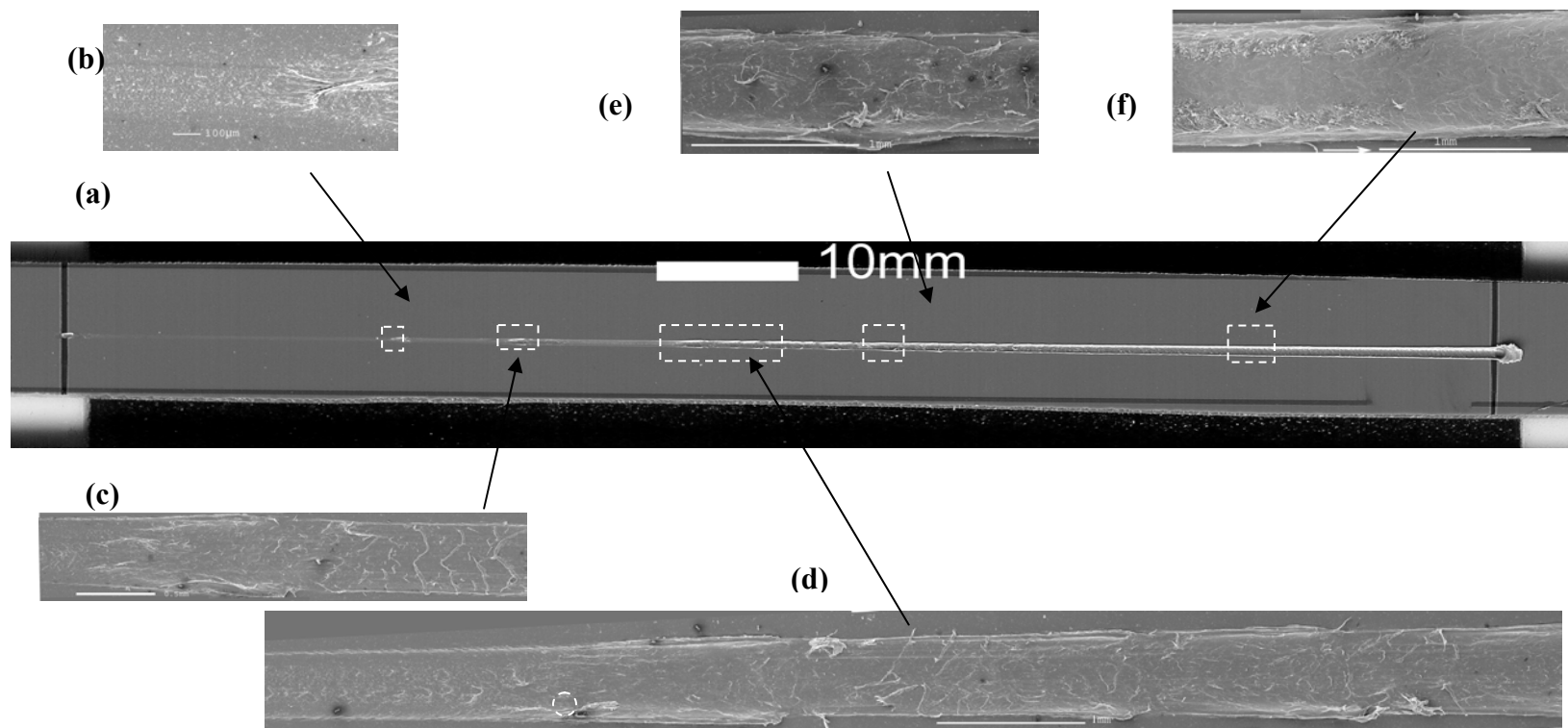


Figure 5.3: (a) Scanned image of scratched talc-filled homopolymer, (b) region 1, (c) region 2, (d) region 3, (e) region 4 and (f) region 5 are SEM micrographs of highlighted regions in the scratch groove. Note that that region 5 shows fibril breakage after sonication.

The scratch distance, which is measured from the start of scratch, of each region shown in Figure 5.2 and 5.3 is recorded. The maximum width in each region was measured using digital image processing software, and the corresponding tangential force and normal load were derived from the frictional plot obtained during testing. Scratching coefficient of friction and scratch hardness is calculated and tabulated in Table 5.1. A comparison of both materials reveals some interesting trends. It is observed that scratching coefficient of friction increases with scratch distance in both homopolymer and talc-filled homopolymer; whereas the opposite is true for scratch hardness. However, the decrease in scratch hardness is much more drastic in talc-filled homopolymer. Although talc allows the polymer to resist deformation better at small loads, the material rapidly degrades and becomes weaker. The reason for such a behavior is discussed in later sections.

Table 5.1: Significant parameters of highlighted regions in Figures 5.2 & 5.3.

Homopolymer						
Region	Scratch Distance (mm)	Width (mm)	Tangential Force (N)	Normal Load (N)	Scratching Coefficient of Friction	Scratch Hardness H_s (MPa)
1	23.80	0.368	2.82	16.6	0.17	156
2	28.09	0.414	2.94	18.7	0.20	139
3	50.90	0.539	8.94	29.8	0.35	130
4	59.36	0.616	8.90	33.9	0.26	114
5	68.7	0.600	12.9	38.5	0.30	128
Talc-filled Homopolymer						
Region	Scratch Distance (mm)	Width (mm)	Tangential Force (N)	Normal Load (N)	Scratching Coefficient of Friction	Scratch Hardness H_s (MPa)
1	23.22	0.243	2.68	16.5	0.16	355
2	31.39	0.430	4.87	20.5	0.24	141
3	43.40	0.497	7.68	26.5	0.29	119
4	58.57	0.608	8.84	33.9	0.26	117
5	91.5	0.746	20.6	50.2	0.41	115

The observed softening of the polymer under higher loads is contrary to intuition. In metals, hardness is expected to increase with normal load due to work hardening [4,50]. In addition, Equations 2.4 and 2.5 implies a quadratic relationship between normal load and indentation width for a spherical indenter indenting under quasistatic conditions, provided that $n = 2$. Scratch hardness is expected to at least remain constant if work hardening does not take place. However, no such simple relationship can be found in this case. Stick-slip motion might be a possible reason for such a behavior. It is observed that stick-slip involves a buildup of stress and gross plastic deformation in front of the tip (see Section 5.3.5), followed by a sudden release of strain energy. This renders Meyer's law invalid because the load bearing area is no longer simply related to d^2 . Figure 5.4 shows the data obtained by measuring the width of the scratch groove as shown in the SEM images in Figures 5.2 and 5.3. Measurements from Region 3 of homopolymer and talc-filled homopolymer are presented here. It can be seen that the stick-slip events are denoted by the spikes in width. It is noted that the scratch width of homopolymer is less than talc-filled homopolymer, which contradicts the findings in Figure 4.8. This is because of the difficulty in defining the peaks of the pileup on both sides of the scratch groove simply by a 2D micrograph. Talc-filled homopolymer tends to produce larger pileups than neat homopolymer, which obscures the actual position of the peaks.

Table 5.2: Mechanical Properties of PP systems

	Tensile Modulus (GPa)	Yield Strength (MPa)
Homopolymer	1.73	33.47
Homopolymer + Talc	2.73	35.30
Copolymer	1.07	22.55
Copolymer + Talc	1.55	23.28

Table 5.2 gives the tensile moduli and yield strengths of the PP systems used. The addition of talc increases both properties when compared to unfilled polymers. This explains in part the large scratch hardness observed initially in talc-filled homopolymer. However, the question as to why its performance degrades so rapidly remains. A possible reason is due to the skin-core morphology that is present in the PP system used in the current study. Skin-core is formed in injection-molded thermoplastics. A faster cooling rate exists next to the mold surface, this induces the polymer in the outer skin to form amorphous phase preferentially, whereas large crystallites and possibly, spherulites are formed in the core of the bulk polymer. A transition zone exists between skin and core that is composed of smaller spherulites. The cross-polarized optical micrograph in Figure 5.5 illustrates an example of skin-core morphology of the system used. The abovementioned zones are indicated in the micrographs. It is possible that as the scratch progresses and reach deeper into the substrate, the change in hardness reflects the different mechanical properties in the layers. Closer inspection on the depth of each layer as shown in Table 5.3, however, disproves this hypothesis. Firstly, the values obtained for skin depth does not seem to correspond well with the observed scratch depths in each micrograph. It is also well-known that polymer crystalline phase is harder than amorphous phase. Changes in hardness, if any, should show an increment instead of decrement [72].

Table 5.3: Skin-core depths of PP

Material	Skin/Transition Depth (μm)	Transition/Core Depth (μm)
Homopolymer	345.24	594.31
Homopolymer + Talc	729.94	1134.37
Copolymer	231.81	586.91
Copolymer + Talc	429.09	1102.31

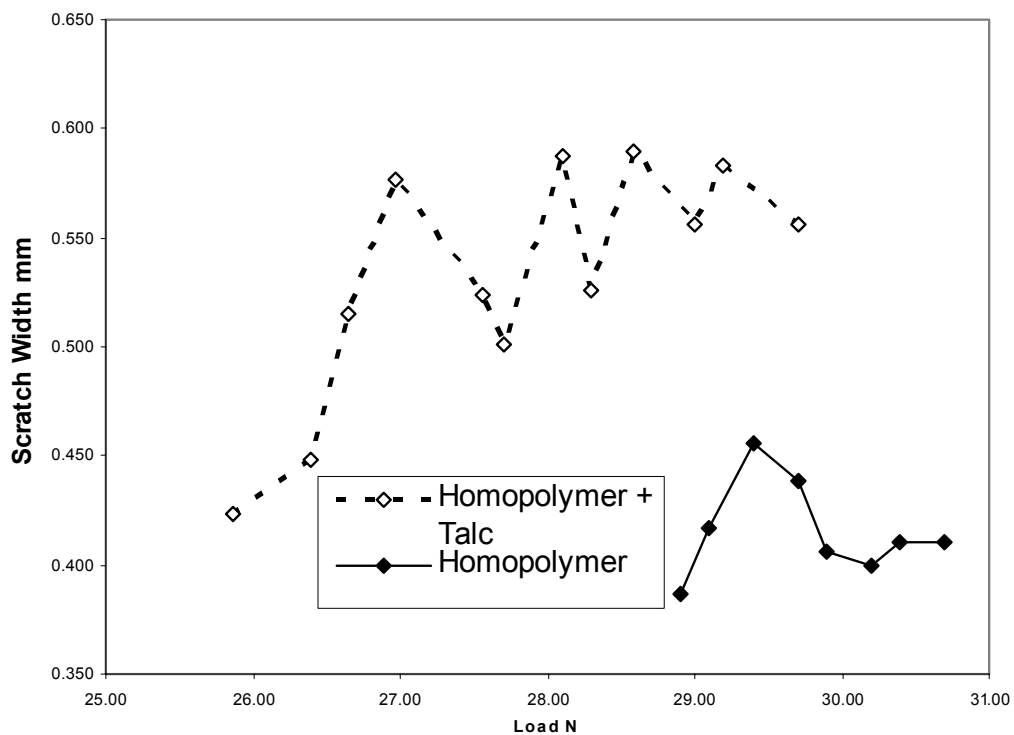


Figure 5.4: Scratch width of regions shown in Figure 5.2 & 5.3. Spikes denote stick-slip events.

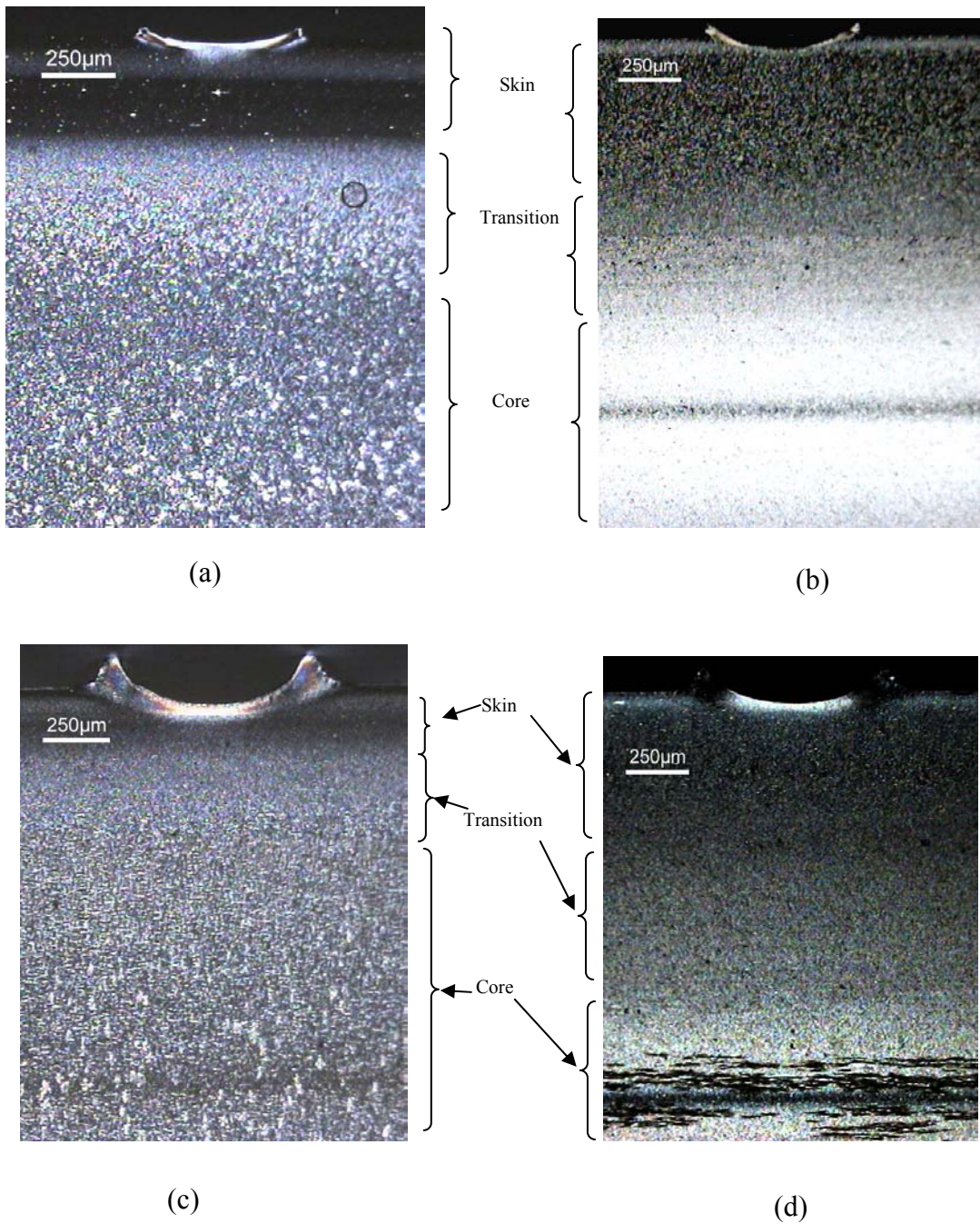


Figure 5.5: Skin-core morphology of (a) homopolymer, (b) talc-filled homopolymer, (c) copolymer and (d) talc-filled copolymer. Note that the cross-section of scratch groove on each surface corresponds to that at 30N normal load.

5.3.2 Scratch Hardness

Scratch widths of the scratched specimens of the four PP systems and polycarbonate were measured from VIEEW[®] direct-light images. Scratch widths from the initial and end regions of the scratch groove were ignored due to instability of scratch in those regions. The projected load-bearing area is then calculated according to the formula, $\pi d^2/4$. The resultant graphs of normal loads against projected load-bearing area were plotted as shown in Figure 5.6. Equation 2.6 suggests that if scratch hardness is constant over a range of loads, then the slope of the linear fit from the above graphs will give the scratch hardness of the material. Indeed, this was the case for the materials tested in this work and all the plots gave very good linear fit. The slope was found easily and the results are shown in Table 5.4. The scratch hardness values from Table 5.4 are in wide disagreement from those found earlier. This disagreement is very likely due to the initial load exerted by the stylus before scratching. The source of this initial load is due to imprecise setting up of initial conditions before scratching. If initial load is zero, the resultant graph will begin at the origin; however, if the initial load is more than zero, the graph will be shifted upwards vertically, as is observed in Figure 5.6. The immediate consequence of this effect is an incorrect scratch hardness when Equation 2.6 is applied to each discrete point. Scratch hardness will be overestimated due to the erroneously steeper than actual slope. Thus the observed softening in scratch hardness found earlier is not real; it is simply due to the inappropriate application of the scratch hardness equation. Employing the graphical method to obtain scratch hardness will eliminate the error induced by the initial load.

The true scratch hardness as shown in Table 5.4 shows the effect of talc on scratch hardness unequivocally. Talc increases scratch hardness in both homopolymer and copolymer PP systems. This is in agreement with the conclusion found in comparing the mechanical properties of the PP systems in Table 5.2. This is a very useful observation, as we can now correlate mechanical properties such as stiffness and

tensile strength with scratch hardness directly. A comparison also shows that the present homopolymer PP systems have comparable scratch resistance to polycarbonate.

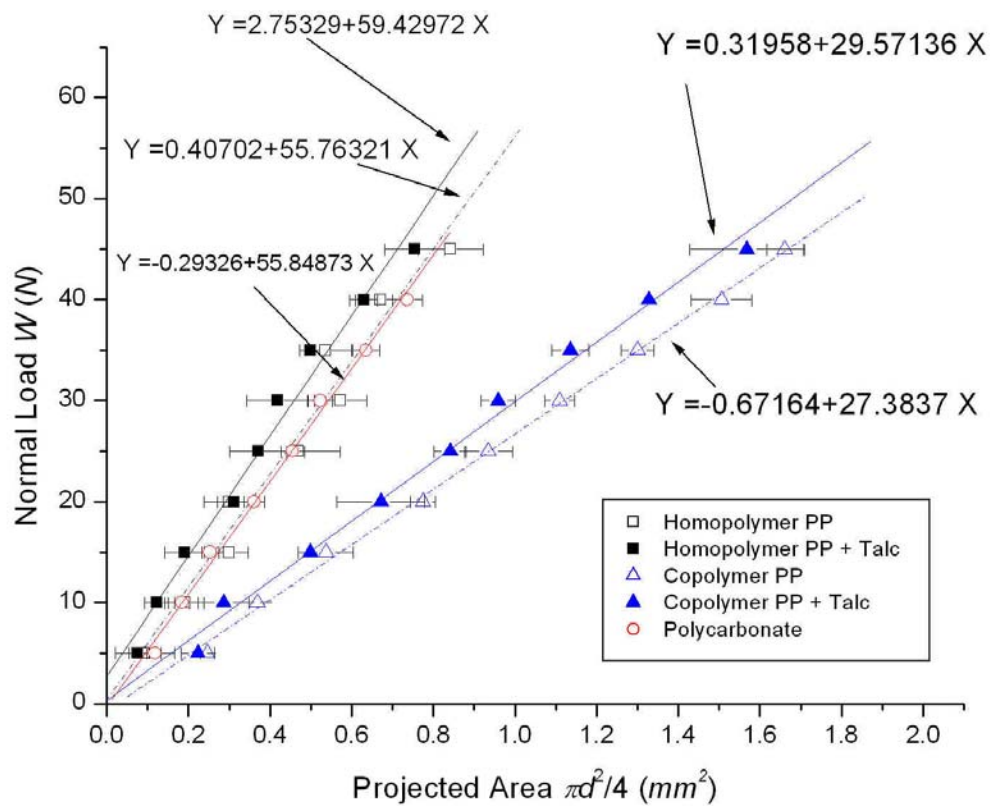
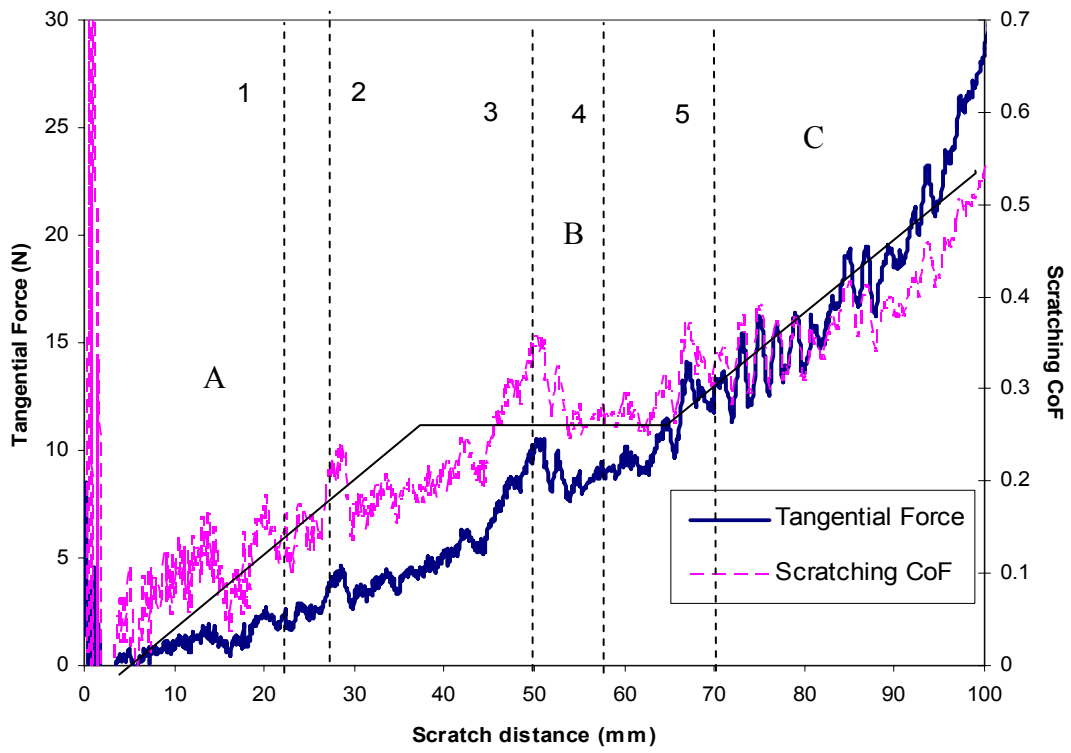


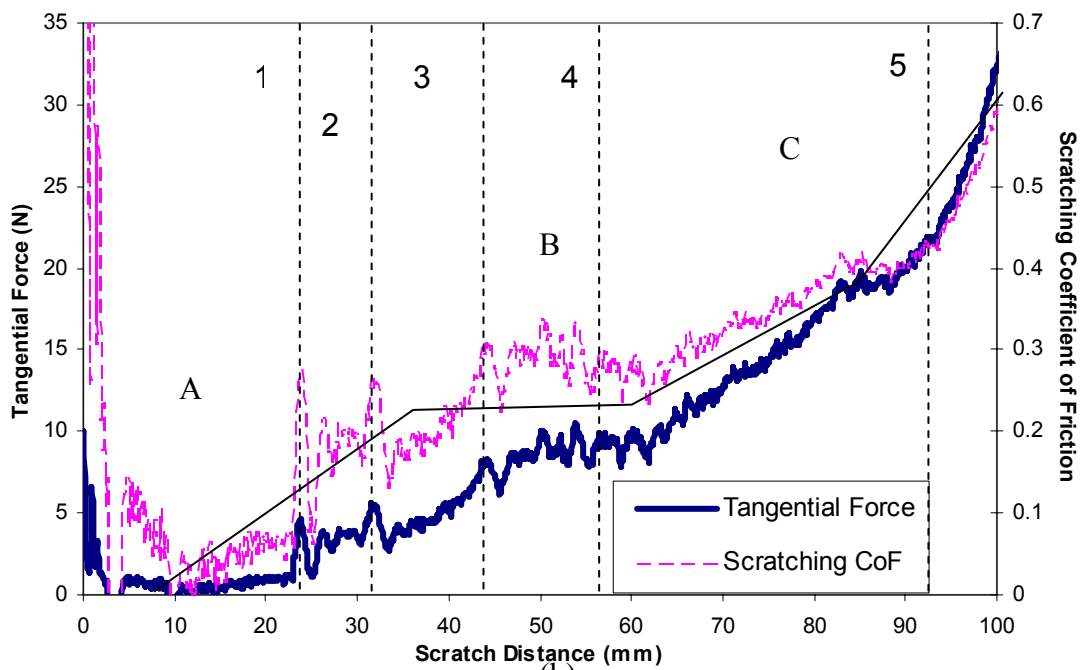
Figure 5.6: Graphical method of obtaining scratch hardness.

Table 5.4: Scratch hardness obtained from graphical method.

Material	Scratch Hardness (MPa)
Polycarbonate	55.8
Homopolymer	55.8
Homopolymer + Talc	59.4
Copolymer	27.4
Copolymer + Talc	29.6



(a)



(b)

Figure 5.7: Frictional force profile from scratch test of (a) homopolymer and (b) talc-filled homopolymer.

5.3.3 Homopolymer Frictional Force Profile

Figure 5.7 (a) and (b) show the frictional force profile for the specimens displayed in Figures 5.2 and 5.3, respectively. Tangential force as measured by the scratch machine is represented by solid lines, while scratching coefficient of friction is represented by dashed lines. The scratching coefficient of friction shows a gradual increase as the scratch distance and normal load increases. A similar behavior was observed in polycarbonate by Rats et al [73]. In their experiments, a Rockwell C type stylus was used to scratch polycarbonate over a load range from zero to ten newtons. This is in clear violation of the First Law of Friction, which is probably due to the fact that such a process violates the basic assumption of no plastic deformation. The usual sense of “coefficient of friction” does not apply here because of this effect. The contribution from the ploughing resistance during scratch becomes significant and the measured “coefficient of friction” is no longer simply a function of interfacial interactions. Thus the term scratching coefficient of friction is used to recognize this distinction.

The profile is characteristically marked by fluctuations that are obviously due to the irregularities encountered during scratching. It is noteworthy to mention here that if the distance, as represented by the dashed vertical lines in the plots, that corresponds to the highlighted regions shown previously in Figures 5.2 and 5.3 are marked on the profile, we can see spikes in some of them. Regions 2 and 3 of Figure 5.2 and Regions 1, 2 and 3 of Figure 5.3 correspond to large spikes in the force profile. Reviewing the SEM micrographs will show that the transitions are sudden, signifying a change in damage mode. This clearly shows the ability of this method to capture important frictional force data that relates to the physical changes during scratch.

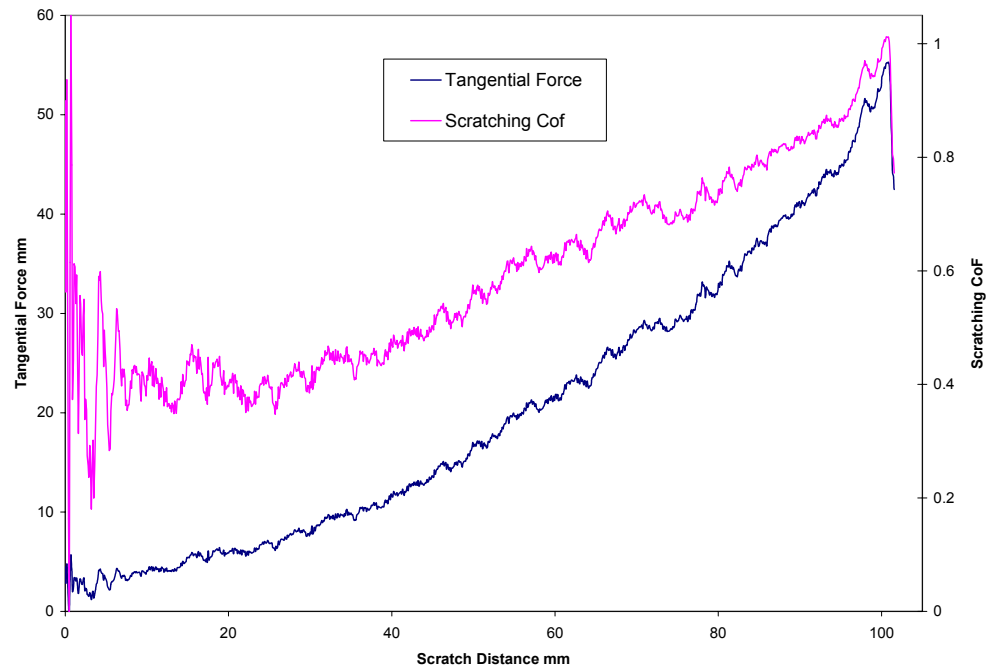


Figure 5.8: Frictional force profile of PC showing constant slope in both curves.

The scratching coefficient of friction is calculated from the linear increase in normal load and the tangential force recorded, derived via Equation 2.7. This second plot is useful in contrasting the spikes and fluctuations that exist in the frictional force plot. The plot is marked initially by instabilities that occur during the start of the scratching process, hence resulting in exaggerated spikes as seen in the plot. The graph stabilizes rapidly and produces a predictable trend. It is noted that there seems to be distinct regions in the profile as scratch progresses. Straight lines are overlaid onto the plot to better distinguish the three distinct regions shown in Figure 5.7(a). Region A denotes a gradual increase in scratching coefficient then it approaches a gentler slope in Region B, which leads to another change in slope in Region C. This curve fitting when coupled with the observations in the SEM micrographs suggests that the varying rate of increase in scratching coefficient is the result of different physical damage mode

occurring during scratch. However, it should be cautioned that the above results should not be construed as evidence that the profile actually increases linearly in each phase, nevertheless it serves as a useful tool in understanding the scratch behavior. For comparison purposes, the frictional profile of a polycarbonate (PC) specimen is shown in Figure 5.8. The scratch groove of the PC specimen showed no transition at all and smooth ploughing took place over the entire scratch length. The scratch test was done under identical conditions as PP. The frictional force plot shows a constant slope over the entire scratch process.

5.3.4 Copolymer Surface Features

The frictional profiles of the scratched PP system thus seem to show a behavior that is incongruent with any previously known theory. To explain the apparent change in the slope of the scratching coefficient, copolymer and talc-filled copolymer systems were sonicated. It is hypothesized that localized regions of the scratched surface are highly strained during the scratch; a controlled burst of energy supplied by the vibration of water during sonication might be able to induce failure in these regions. It was hoped that the copolymer systems, having a lower stiffness and higher ductility, will show sonication-induced failure more readily. Copolymer does not show any induced failure from the sonication (Figure 5.9). Region 1 shows a gradual transition from regularly spaced wave-like lines, due to formation of shear bands, to irregular deformation lines. Region 2 shows extensive deformation that marks the beginning of the stress-whitened zone.

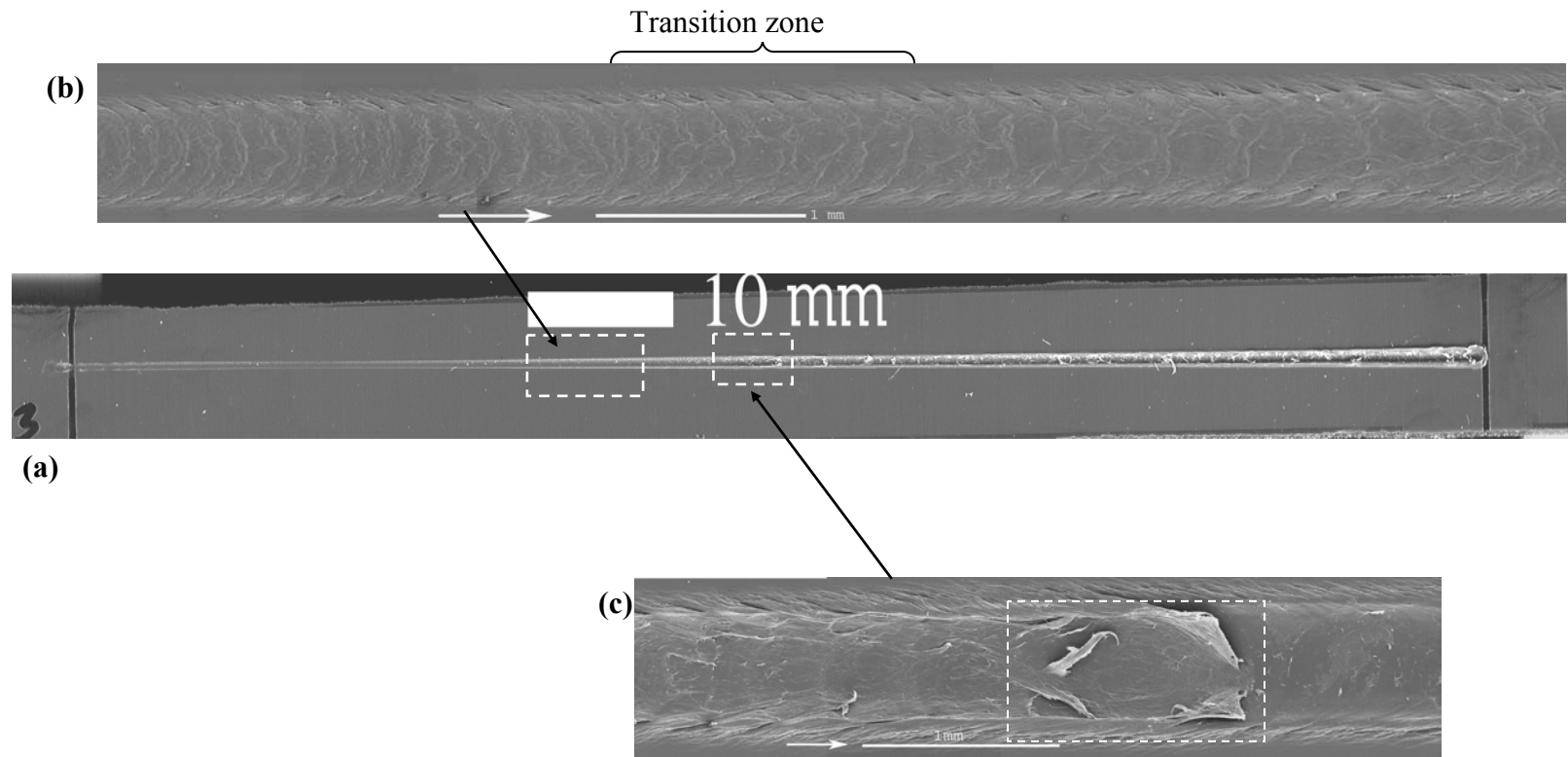


Figure 5.9: (a) Scanned image of scratched copolymer that was sonicated, (b) region 1 and (c) region 2 shows extensive deformation indicated by box.

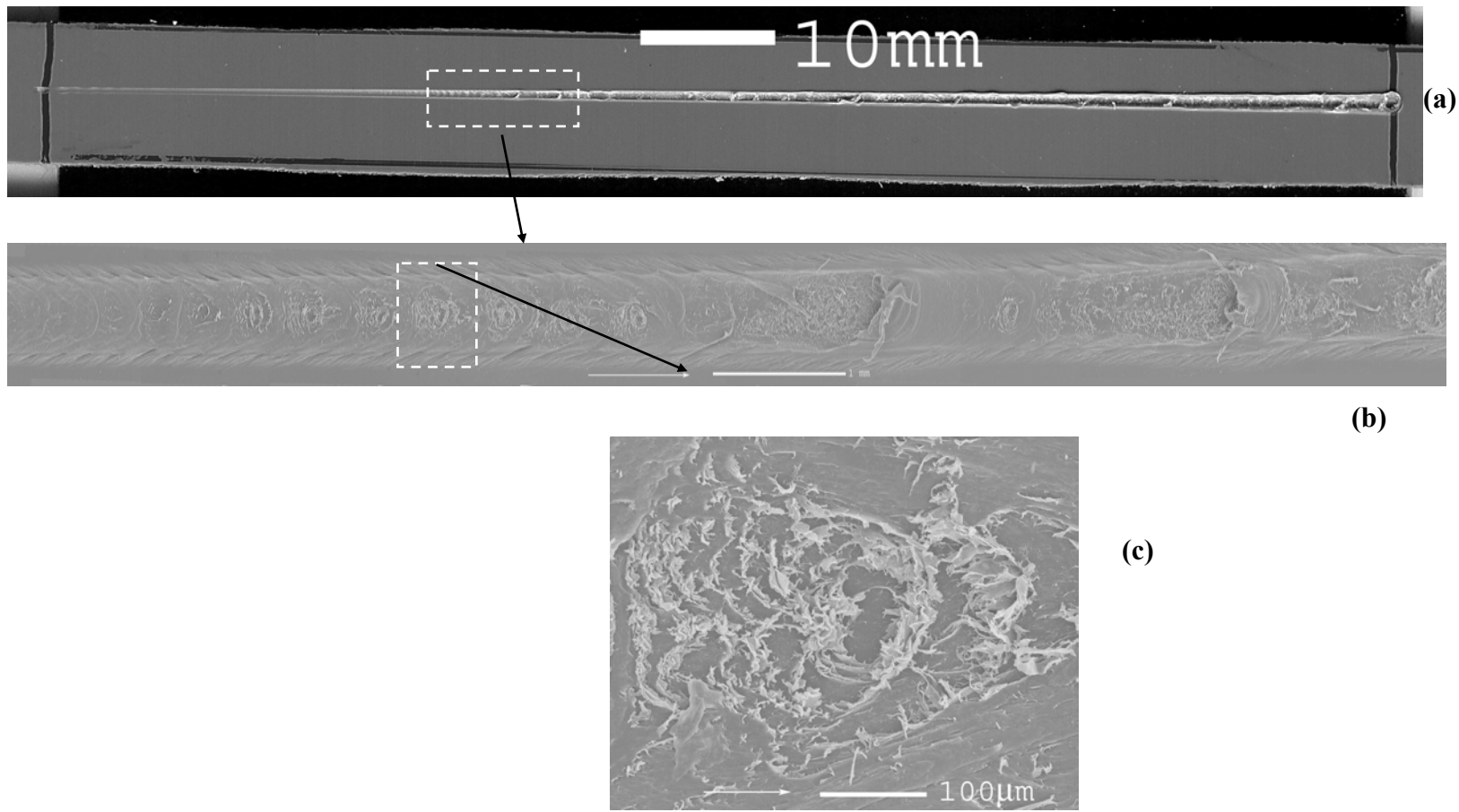


Figure 5.10: (a) Scanned image of scratched talc-filled copolymer that was sonicated, (b) region 1 and (c) close up of a pit in region 1.

Talc-filled copolymer, however, shows a very different surface feature after sonication. Figure 5.10 shows the appearance of pits on the surface that correspond to highly visible marks in the scanned image. The pits exhibit remnants of broken fibrils at the edges. The pits appear to be made up of concentric circles of layers of polymer. In fact, the step-like features allows easy counting of the number of layers in each pit. As the scratch progresses, the pit grows by increasing the number of steps. Eventually the pits give way to large scale failure that creates the feature seen on the right of the pits. It is of significance to note that the substrate material forms layers, each with a different amount of stretching during the scratch process. It is proposed that this process is similar to the biaxial stretching of polymer films. The inter-pit distance is plotted and the data shown in Figure 5.11. It is apparent that inter-pit distance increases with increasing scratch distance, which accounts for the larger deformation observed as scratch distance increases.

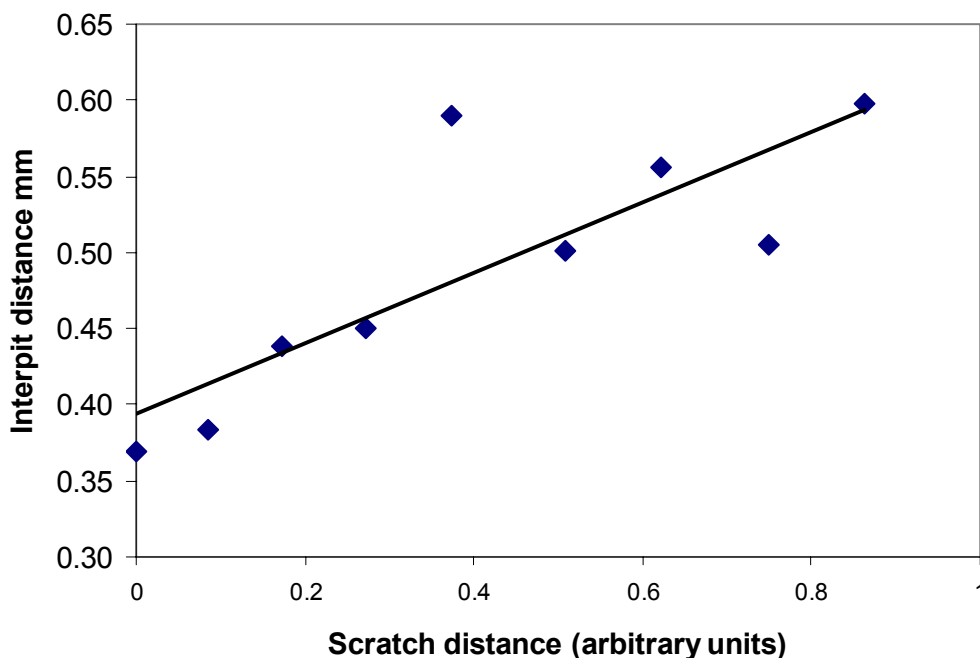
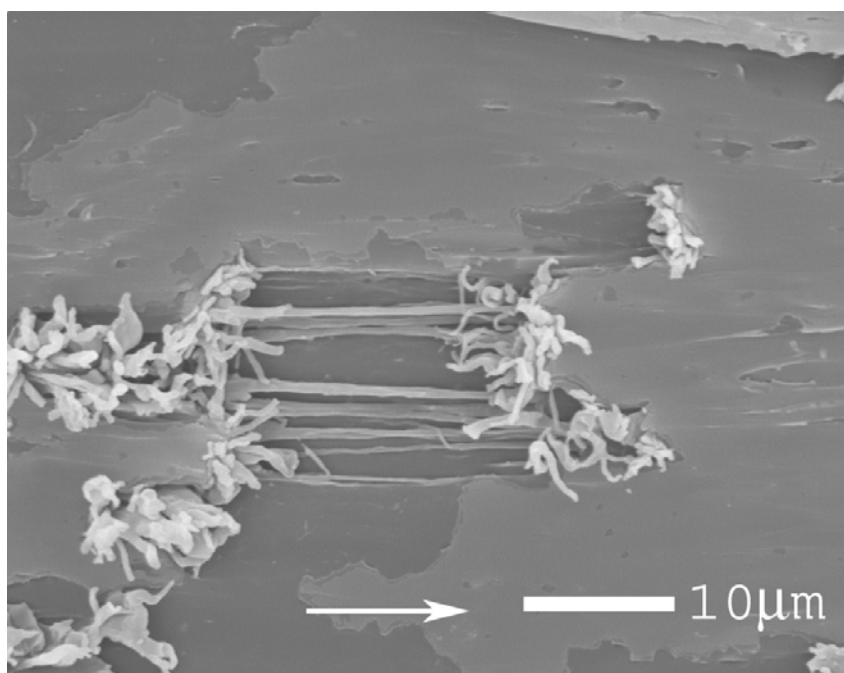
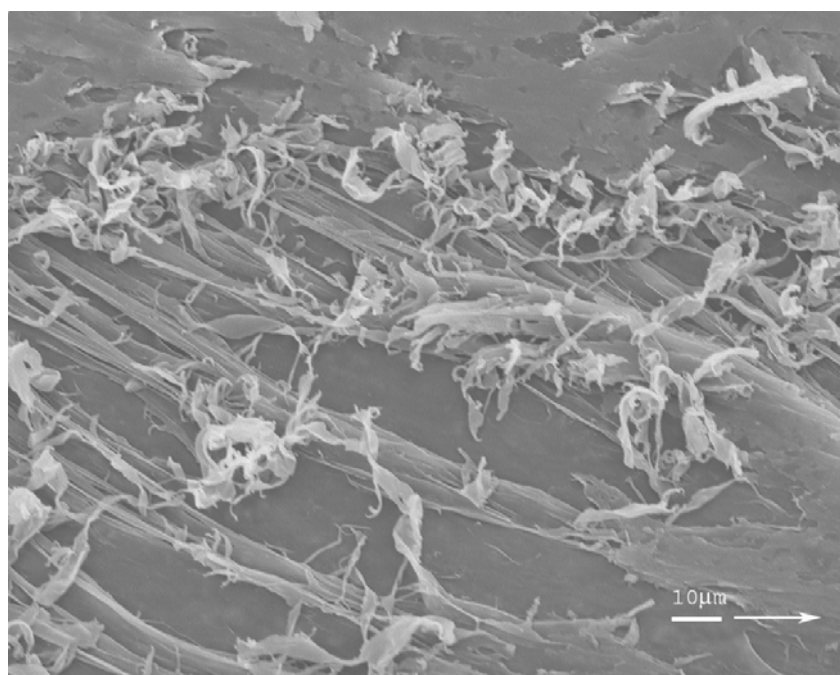


Figure 5.11: Inter-pit distance shows an increase against scratch distance.

Encouraged by the results shown in talc-filled copolymer, the homopolymer systems were revisited and sections that correspond to the later portion of the scratch were also sonicated. It is anticipated that sections under higher loads should provide a better chance in showing highly strained regions. It is found in Figures 5.2(f) and 5.3(f) that remnants of broken fibrils were formed on the side walls of the groove. This indicates that the region most highly strained in homopolymers are on the side of the groove, in contrast to copolymers, where the most strained regions are at the center of the groove. Figure 5.12 (a) and (b) show the formation of fibrils in homopolymer and talc-filled homopolymer, respectively. The presence of fibrils offers another explanation to the observed change in coefficient of friction of PP. Fibrils are formed during cold-drawing of the polymer. Figure 5.13 shows a tensile engineering stress-strain graph typical of a material that yields and cold-draw. Cold-drawing occurs within the plateau region. It can be seen that stress remains relatively constant while strain increases dramatically within this region.

**(a)****(b)****Figure 5.12:** Fibrils in (a) homopolymer and (b) talc-filled homopolymer.

5.3.5 Copolymer Frictional Force Profile

Frictional force profile for copolymer systems is in general similar to that of homopolymer systems. Four distinct regions can be seen and they behave in a similar manner as mentioned in section 5.3.3. Figure 5.14(a) and (b) shows the frictional force profile of copolymer and talc-filled copolymer respectively. Regions 1 and 2 shown in Figure 5.9 are marked in 5.14(a). Region 2 shows a spike that corresponds to the observed deformation event. Figure 5.14(c) shows the detailed profile of (b) that corresponds to the surface features observed in Figure 5.10(b). Each dashed line in the cluster of lines on the left of the graph indicates a pit in the SEM. It can be seen that each pit corresponds to a peak in the frictional force profile. There is an unaccounted spike in between the ninth and tenth line that does not appear to correspond to any physical feature observed. The two larger peaks on the right of the graph correspond to the two large-scale deformation regions observed in the SEM. Thus the above results further corroborates that the pits are the highly strained regions. The fidelity of the frictional force profile to the SEM images is also demonstrated in this study.

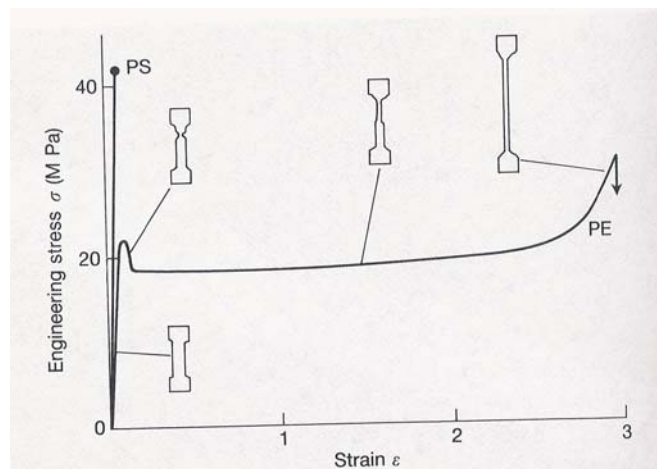
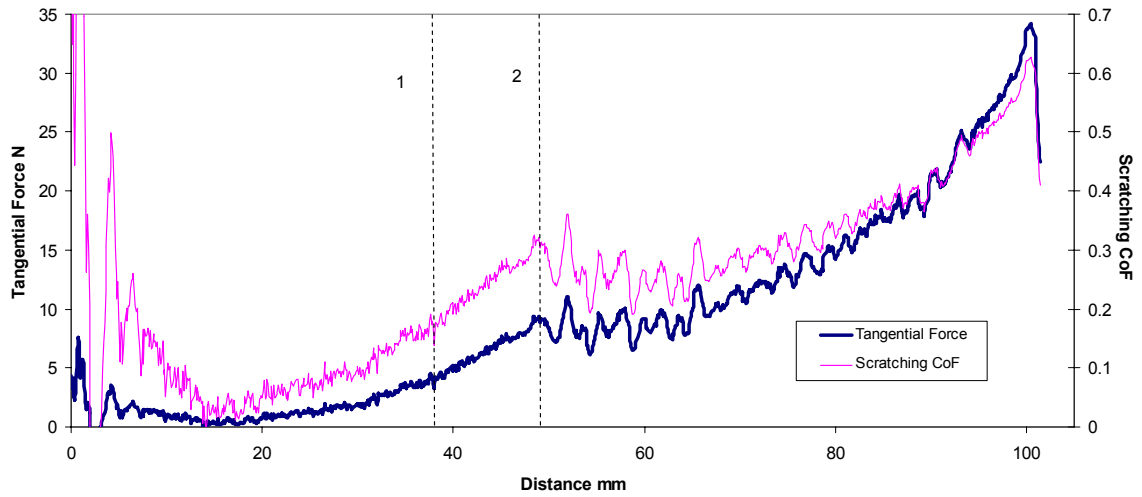
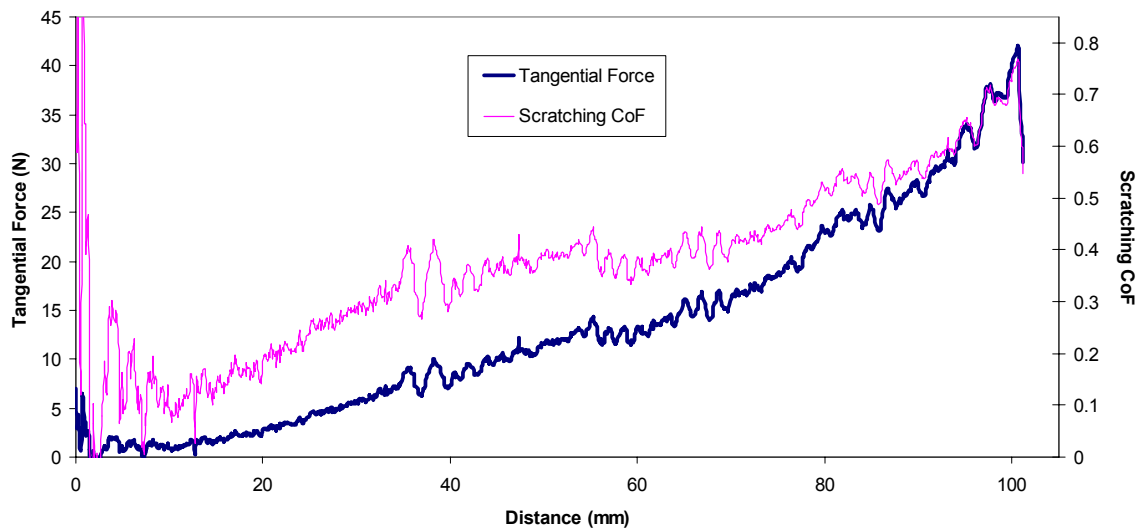


Figure 5.13: Engineering stress-strain graph of a material that yields and cold-draws. (after McCrum et al. [74])



(a)



(b)

Figure 5.14: Frictional force profile from scratch test of (a) copolymer and (b) talc-filled copolymer. (c) shows the detailed profile of (b) that corresponds to Figure 5.10 (b).

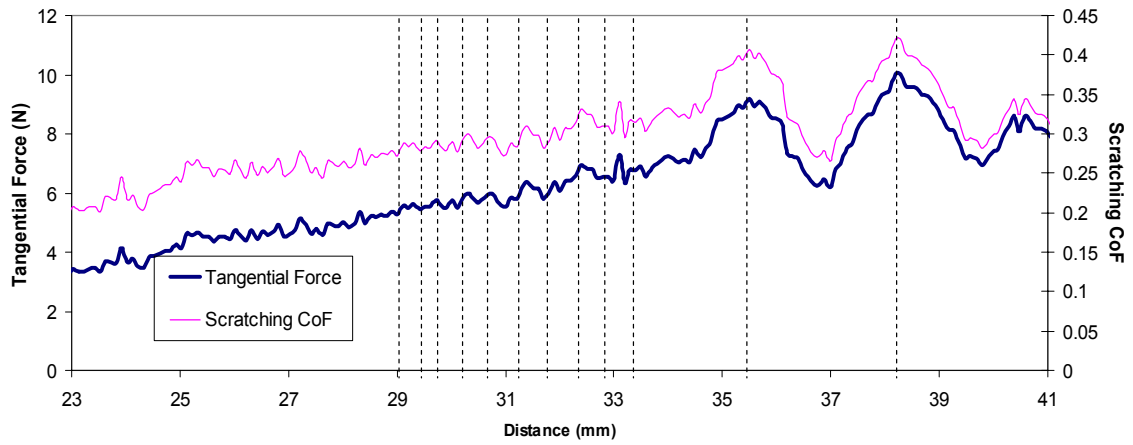


Figure 5.14. Continued

(c)

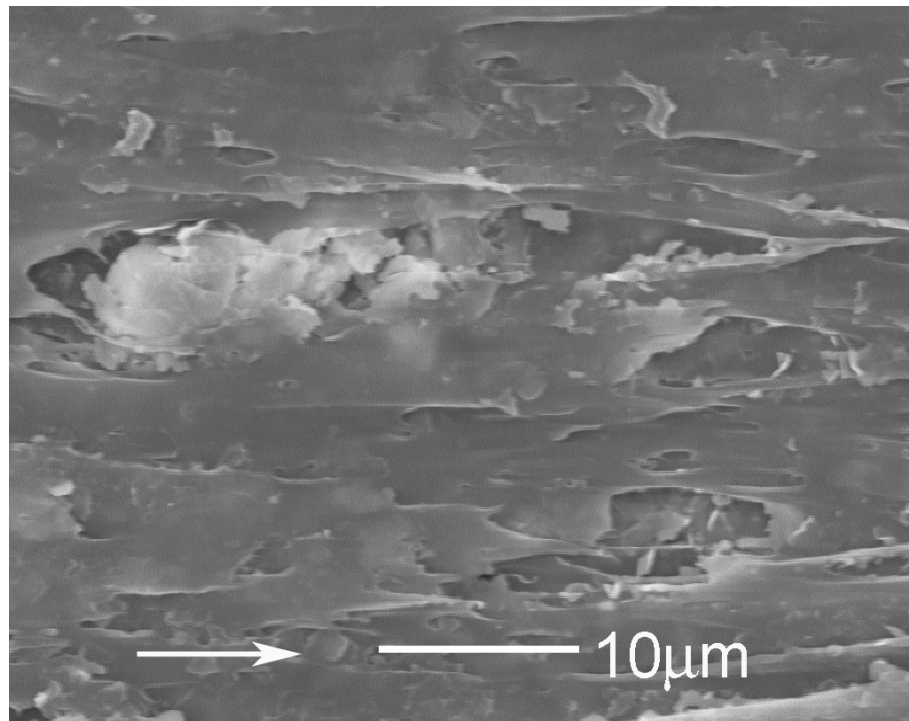


Figure 5.15: SEM micrograph of exposed talc particles in a talc-filled homopolymer. Arrow indicates scratch direction.

5.3.6 Scratch Visibility

5.3.6.1 Stress-whitening

It is well-known that crazing produces voids which could contribute to stress whitening. Rengarajan et al. [75] found that PP which contained impact modifiers that promote shear deformation exhibits less stress-whitening than PP containing impact modifiers that promote crazing and void formation. Tang and Martin [71] had provided evidence of void nucleation from the rubber phase in PP. The current copolymer actually contains a rubber phase, and thus stress-whitening can occur either by voiding or crazing induced by the rubber phase. This explains why the copolymer system has a lower critical load to onset of stress-whitening. A stronger rubber phase-matrix bonding may reduce the nucleation of voids and stress-whitening.

Talc, if not properly modified, is well-known to increase stress-whitening of polymers. The SEM micrograph in Figure 5.15 shows exposed talc particles after scratch at 30 N and 100 mm/s in the homopolymer. Figure 5.16 (a) shows an image that was obtained from VIEEW[®]. Blue and green diffuse light were used during the scanning of the images as it was found that visibility of the scratch grooves in talc-filled systems were most prominent at these particular wavelengths. Holoubek et al.[59] showed that in a stress-whitened polypropylene, light scattering due to voids is relatively insensitive to different wavelengths of the visible light. Whereas, light scattering due to ethylene-propylene-diene monomer (EPDM) rubber particles embedded in polypropylene is most effective at wavelengths around 400 nm (violet), which gradually drops off as wavelength increases. Although talc particles, not EPDM particles, are present in the talc-filled homopolymer PP, the fact that scratch visibility is sensitive to wavelength of light suggests that talc plays an important role in causing such pronounced increase in scratch visibility.

The highlighted region in Figure 5.16(a) represents the area that was stress-whitened. When this image is superimposed onto the frictional force profile, a correlation between the onset of stress-whitening and a steep drop in frictional force is easily seen. This coincidence in onset of stress-whitening and drop in frictional force is observed in all polymer systems except for homopolymer PP, where no appreciable stress-whitening was detected. Another feature that seems to be recurring is the higher probability of large amplitude fluctuations that manifests after this steep drop in friction. The large fluctuations would seem to suggest that the damage mechanism has changed such that a smooth sliding motion across the surface becomes less likely. Yielding, fracture or stick-slip events as evidenced in the earlier micrographs are possible reasons for the observed fluctuations. The drop in friction is probably a result of a sudden failure by yielding or fracture, which can result in the formation of voids or exposure of talc particles. It has been suggested that talc particles in PP play no role in shear band formation during scratch [71]. In the present case, the presence of talc particles aggravates the damage by the debonding of particle-matrix interface and matrix drawing, as seen in Figures 5.3 and 5.15.

A set of three specimens from each material was scanned using the VIEEW[®] system, the critical load to onset of stress-whitening was obtained and the results are given in Figure 5.17. The results show that the magnitude of critical load to stress-whitening occurs in the following descending order: homopolymer, talc-filled homopolymer, copolymer, talc-filled copolymer. We see that scratch visibility is partly dependent on mechanical properties, such as tensile modulus and yield strength (Table 5.2). Lower moduli and lower yield strength give a lower critical load for unfilled PP systems. Figure 5.18 shows the size of the area that was stress-whitened for each material system. Talc-filled polymers show a larger affected area. It is apparent that talc not only decreases the critical load to stress-whitening, it also dramatically increases the amount of stress-whitening.

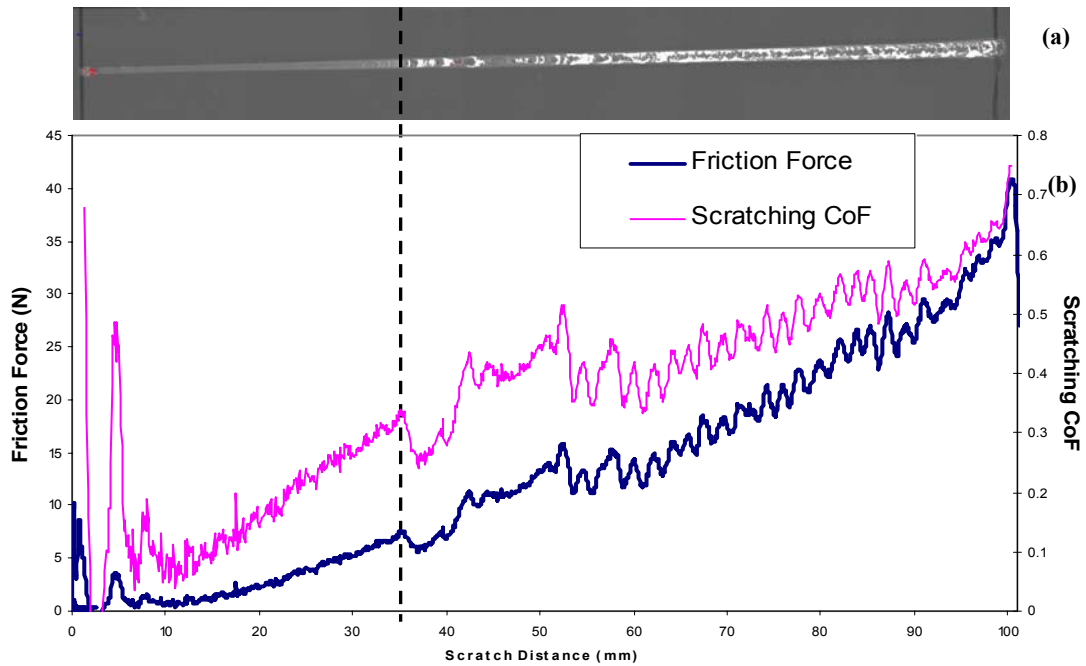


Figure 5.16: (a) Image from VIEEW[®], white region indicates stress-whitening, (b) frictional profile for this talc-filled copolymer specimen, dashed line shows excellent correlation with onset of stress-whitening.

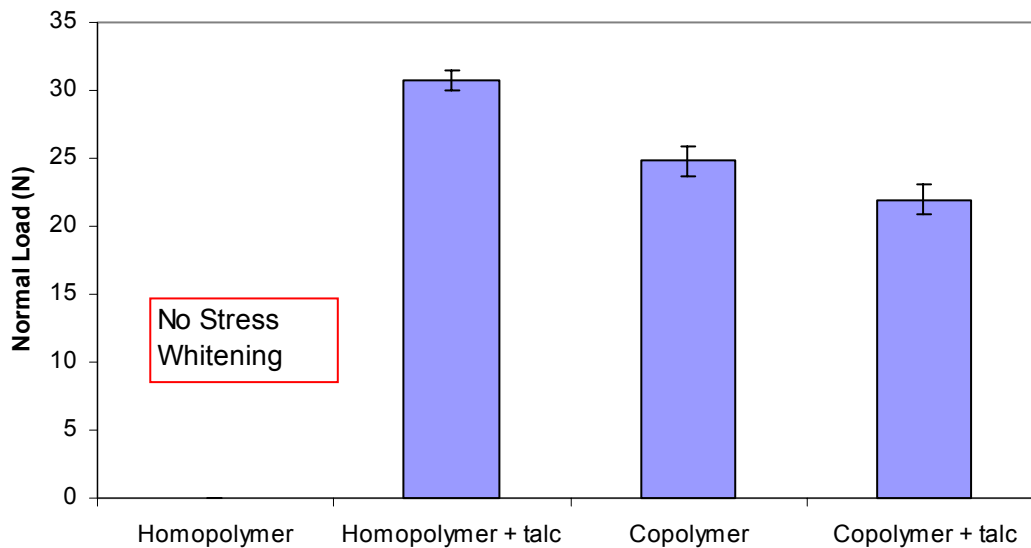


Figure 5.17: Critical load to onset of stress-whitening.

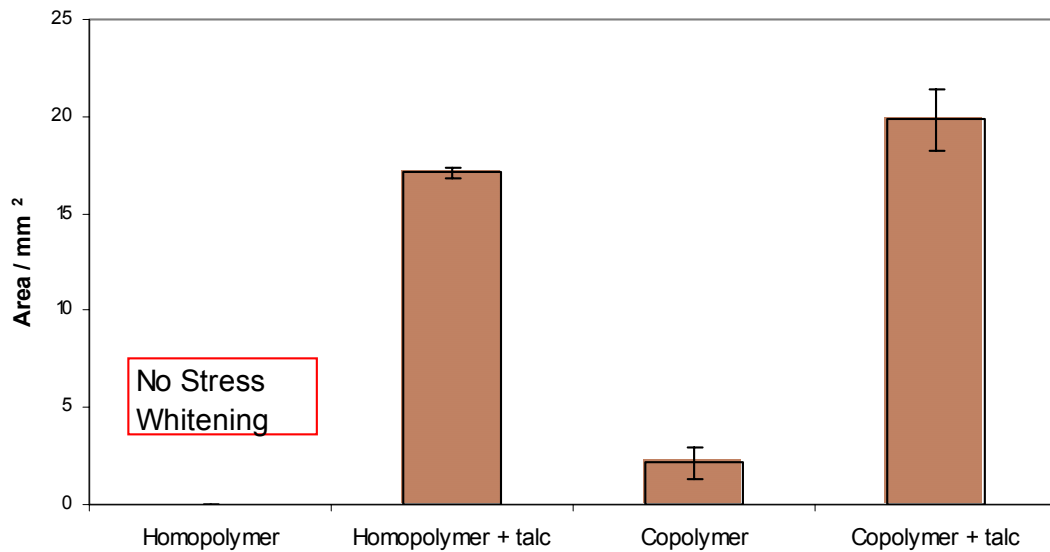


Figure 5.18: Area of scratch groove that was stress-whitened.

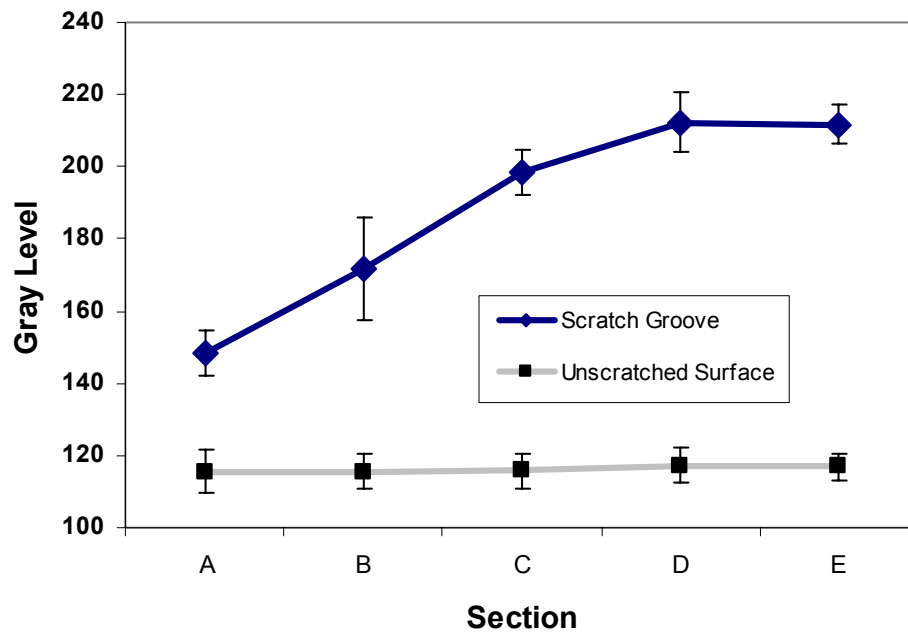


Figure 5.19: Gray level plot of scanned image of a copolymer *via* flatbed scanner.

The evidence presented points strongly to the role of filler particles in scratch visibility. It is thus proposed that the real reason for the difference in scratch visibility between the current PP materials used is the tendency of the material to form light scattering voids or to expose talc particles at the critical load. Logically, this load will probably be dependent on some yielding or fracture criteria, depending on the specific failure mode that occurred. To illustrate this point, homopolymer is found to fail by fracture without any observable voids (Figure 5.2). On the other hand, talc-filled homopolymer fails *via* debonding of talc particles and drawing of the matrix as evidenced. Voids and debonding occur as a direct consequence of this change in damage mode, and these are the causes for significant light scattering. Accordingly, for homopolymer PP, it is suggested that minimal stress-whitening will take place as long as the failure mode do not change. The approach to the reduction of scratch visibility can be partially answered. Preventing the material from reaching a deleterious mode of failure, *i.e.*, extensive fibrillation of the matrix or debonding should reduce scratch visibility. This can be achieved by applying hard coats on top of the polymer, by using polymers with high yield strength and fracture strength, or by improving interfacial strength between filler particle and polymer matrix.

Figure 5.19 presents the gray level analysis via scanner method described earlier. A graph of the gray levels of unscratched surface was plotted to contrast that of the scratch groove. The graph of the unscratched surface remains constant throughout the scratch length, while the scratch groove shows a gradual increase in gray level. Owing to the fact that the scanner can only show a monotonic increase without any prominent peaks or change in value, it will not be very useful in characterizing scratch visibility.

5.3.6.2 Ductile vs. Brittle Failure

The present work suggests that stress-whitening is mainly due to the surface drawing of the scratched polymer. The ductile drawing is caused by void formation and debonding of rubber phase and talc particles from the matrix. Evidence of large tracts of material being removed (peeling) can also be seen in Figures 5.9(c) and 5.10(b). In contrast, materials that failed in a localized brittle manner, i.e., homopolymer and talc-filled homopolymer, display minimal stress-whitening. Previous work done by other authors, such as Lin et al. [76] and Bertrand-Lambotte et al. [38], support the view that brittle failure will increase scratch visibility. It is reasoned that brittle failure will increase surface roughness of the scratch groove because of the formation of cracks, while ductile failure gives a smooth polished surface. Subsequently, as the eye is more sensitive to the change in surface roughness, scratch visibility is increased. However, it must be noted that the aforementioned authors came to this conclusion from scratch tests done on automotive clearcoats that produces scratch deformation in the microscale range of up to 20 μm . Thenceforth, it is applicable to situations where marring occurs, an example being mars produced by minuscule sand particles. In the present case, where the dominant mechanism that produces large surface roughness is ductile failure due to voiding and debonding, a diametrically opposite conclusion is obtained. These contrasting conclusions show that scratch visibility cannot be described as simply related to ductile or brittle failure. The effect of the mode of failure to scratch visibility is sensitive to the type of material and possibly size of the scratches.

5.4 Conclusions

It has been shown that different surface damage features are present as scratch progresses under linear load increase. The surface damage transitions, such as mar-scratch and stress-whitening, can be correlated to transitions in the frictional force profile and scratching coefficient of friction. Using sonication to induce failure in highly strained regions, it was found that highly strained regions in homopolymers occur on the side of the groove. For copolymers, highly strained regions occur in the center of the groove. Subsurface of polymer appears to form layers when scratched and in talc-filled copolymer under high strain and high stress, the affected zone forms a spherical volume, which manifests as pits after sonication.

High fidelity of the frictional force profile to SEM images was demonstrated. Significant features found in SEM can always be corroborated to the peaks in the frictional force profile. It was found that stress-whitening is always followed by a drop in friction. This observation provides a useful criterion in defining the initiation of stress-whitening in PP. Talc, if not properly modified, was found to have a deleterious role in terms of scratch visibility, even though it increases scratch hardness. Talc is responsible for lowering the critical load to onset of stress-whitening and for increasing the amount of stress whitening. Based on the observations in the present paper, it is suggested that to reduce scratch visibility, it requires the suppression of undesirable failure mechanisms during scratch, such as localized plastic drawing and debonding of filler particles.

VIEEW[®] was found to be a useful method in quantifying scratch visibility. The critical load to the onset of stress-whitening can be found easily. It was also found that localized ductile drawing promotes stress-whitening and thus increases stress visibility.

Critical parameters of scratch were obtained and surface damage study revealed important information regarding scratch damage mechanism. In conclusion, the present test method has been shown to be very useful in characterizing scratch properties of polymers.

CHAPTER VI

CONCLUSIONS

6.1 Summary

In this study, a new scratch test methodology was proposed and evaluated. It was found that the progressive load test was the most useful method. FE analysis was able to correlate experimental results qualitatively well, thus allowing for gaining fundamental knowledge using FE modeling. Tests have shown that the progressive load test was able to determine critical values for damage formation during scratching of polymers. Surface studies from the scratched samples indicate that scratch resistance and visibility can be described quantitatively using the corresponding critical load, thus allowing for quantitative and meaningful ranking and comparison among polymers.

It was found that the scratch hardness of PP remains constant at the range of loads used in this experiment. The graphical approach was used to avoid errors induced by the initial load of the scratch stylus. The different materials exhibit distinct scratch hardness values that can be correlated to tensile strength and stiffness. Talc was found to increase scratch hardness, which is similar to the effect seen in tensile strength and stiffness. This method is a useful way to rank materials according to scratch hardness. It is suggested that, based on the evidence presented by sonication-induced failure of the scratch-damage surface, cold drawing of polymers during scratch that homopolymer and copolymer systems have different scratch-induced damage patterns.

It was also found that the present method was able to capture frictional force data accurately. Surface features that indicated transitions in damage mode could be deduced from the frictional force profile alone. In particular, stress-whitening of polypropylene (PP) could be accurately deduced from the scratching coefficient of friction plot. This

has important implications in the study and design of polymers to delay or eliminate stress-whitening. So far, this is the only method known that can correlate stress-whitening of PP due to scratch in a simple test.

Talc, if not properly modified, was found to play an important role in scratch damage behavior of PP. It was found to alter the failure mode during scratch, thereby inducing larger amount of stress-whitening compared to neat PP. It is thought that the major reason for the degradation in scratch resistance is due to the debonding of the particle- polymer interface. It was also found that localized ductile drawing (fibrillation) during scratch would result in more stress-whitening.

It was shown that the effect of the filler is very important and might overcome any benefits that are brought about by increased scratch hardness. It is suggested that to reduce stress-whitening, thereby reducing scratch visibility, particle-matrix interface should be strengthened, particle size should be reduced, and the polymeric matrix should not fail via fibrillation caused by cold drawing during scratching.

6.2 Recommendations for Future Research

The results from this study have led to a better understanding of how PP behaves during scratch. The combination of mechanics and materials science study has been a fruitful endeavor and resulted in giving us a more complete picture of the process of scratch in polymers. The frictional force plot has the potential of becoming an important tool in predicting scratch behavior. The different highly strained damage zones observed in homopolymer and copolymer systems pose an interesting question in the mechanics of scratch in these materials. Further FE modeling should be done to provide an explanation to this phenomenon. It is also recommended that intense study on the frictional force plot of various test conditions and materials be carried out. The effect of lubricant is one possibility that could provide us with more understanding of the scratch

process. Scratching under different temperatures will also be a worthwhile experiment, where ductile-brittle transition of the polymer is expected to produce interesting results. This work has also shown the importance of filler on scratch hardness and scratch visibility. Further work should be done to study the effect of fillers on these two aspects of scratch.

REFERENCES

1. I.M. Hutchings, Tribology — Friction and Wear of Engineering Materials, CRC Press, Boca Raton, 1992.
2. B.N.J. Persson, Sliding Friction – Physical Principles and Applications 2nd Edition, Springer, Berlin, 2000.
3. A.K Geim, S.V. Dubonos, I.V. Grigoreiva, K.S. Novoselov, A.A. Zhukov, S. Yu. Shapoval, Microfabricated adhesive mimicking gecko foot-hair, Nature Materials, 2 (2003) 461–463.
4. D. Tabor, The Hardness of Metals, Oxford University Press, Oxford, 1951.
5. B. J. Briscoe, K. S. Sebastian, The elastoplastic response of poly(methyl methacrylate) to indentation, Proc. R. Soc. Lond. A 452(1946) (1996) 439-457.
6. M. Sakai, Y. Nakano, Elastoplastic load-depth hysteresis in pyramidal indentation, J. Mater. Res. 17(8) (2002) 2161-2173.
7. A. C.-M. Yang, T. W. Wu, Wear and friction in glassy polymers: microscratch on blends of polystyrene and poly (2,6-dimethyl-1,4-phenylene oxide), J. Polym. Sci. B: Polym Phys. 35 (1997) 1295-1309.
8. R. Rikards, A. Flores, Numerical modeling of microhardness tests for polymer materials, J. Macromol. Sci. Phys. B 40(5) (2001) 763-774.
9. B.J. Briscoe, P.D. Evans, S.K. Biswas, S.K. Sinha, The hardness of poly(methylmethacrylate), Tribol. Intern. 29(2) (1996) 93-104.
10. H. C. Y. Cartledge, C. Baillie, Y-W. Mai, Friction and wear mechanisms of a thermoplastic composite GF/PA6 subjected to different thermal histories, Wear 194 (1996) 178-184.
11. F.P Bowden, D. Tabor, The Friction and Lubrication of Solids Part II, Oxford University Press, Oxford, 1964.
12. P.R.J. Guevin, State-of-the-art instruments to measure coating hardness, J. Coat. Technol. 67 (840) (1995) 61-65.

13. T. Triplett, Two-component: the magic's in the mix, *Ind. Paint Powder* 72 (4) (1996) 34-37.
14. F. Ramsteiner, T. Jaworek, M. Weber, S. Forster, Scratch resistance and embrittlement of coated polymers, *Polym. Test.* 22 (2003) 439-451.
15. B.J. Briscoe, P.D. Evans, E. Pelillo, S.K. Sinha, Scratching maps for polymers, *Wear* 200 (1996) 137-147.
16. B.J. Briscoe, E. Pelillo, S.K. Sinha, Scratch hardness and deformation maps for polycarbonate and polyethylene, *Polym. Eng. Sci.* 36(24) (1996) 2996-3005.
17. B.J. Briscoe, E. Pelillo, F. Ragazzi, S.K. Sinha, Scratch deformation of methanol plasticized poly(methylmethacrylate) surfaces, *Polymer* 39(11) (1998) 2161-2168.
18. B.H. Stuart, B.J. Briscoe, Scratch hardness studies of poly(ether ether ketone), *Polymer* 37(17) (1996) 3819-3824.
19. G. Gauthier, R. Schirrer, Time and temperature dependence of the scratch properties of poly(methylmethacrylate) surfaces, *J. Mater. Sci.* 35 (2000) 2121-2130.
20. P.Z. Wang, I.M. Hutchings, S.J. Duncan, L. Jenkins, Quantitative characterization of scratch damage in polypropylene (TPO) for automotive interior applications, *SAE Transactions* 1999-01-0243 (1999) 134-150.
21. B.Y. Ni, A.L. Faou, Scratching behaviour of polymer films using blunt spherical styli, *J. Mater. Sci.* 31 (1996) 3955-3963.
22. A. Krupička, M. Johansson, Use and interpretation of scratch tests on ductile polymer coatings, A. Hult, *Prog. Org. Coat.* 46 (2003) 32-48.
23. Micro Photonics Inc., CSM Revetest Scratch Tester, July 2003, <http://www.microphotonics.com/revetest.html>.
24. J. Chu, L. Rumao, B. Coleman, Scratch and mar resistance of filled polypropylene materials, *Polym. Eng. Sci.* 38(11) (1998) 1906-1914.
25. J. Chu, C. Xiang, H.-J. Sue, R.D. Hollis, Scratch resistance of mineral-filled polypropylene materials, *Polym. Eng. Sci.* 40(4) (2000) 944-955.

26. J. Chu, Scratch resistance of PP composites, 43rd International SAMPE Symposium (1998) 1149-1157.
27. J.R. Grasmeyer, Scratch-resistant polypropylene compounds, Institute of Polymer, Polypropylene, the International Conference (1994) 98-108.
28. R.S. Kody, D.C. Martin, Quantitative characterization of surface deformation in polymer composites using digital image analysis, *Polym. Eng. Sci.* 36(2) (1996) 298-304.
29. A. Chanda, D. Basu, A. Dasgupta, S. Chattopadhyay, A.K. Mukhopadhyay, A new parameter for measuring wear of materials, *J. Mater. Sci. Lett.* 16 (1997) 1647-1651.
30. M. Coulon, W. Lenne, Scratch resistance of optical polymers, *Polym. Test.* 2 (1981) 199-210.
31. B.J. Briscoe, A. Delfino, E. Pelillo, Single-pass pendulum scratching of poly(styrene) and poly(methylmethacrylate), *Wear* 225-229(1) (1999) 319-328.
32. O. Vingsbo, S. Hogmark, Single-pass pendulum grooving- a technique for abrasive testing, *Wear* 100 (1984) 489-502.
33. Y.N. Liang, S.Z. Li, D.F. Li, S. Li, Some developments for single-pass pendulum scratching, *Wear* 199 (1996) 66-73.
34. B. Lamy, Effect of brittleness index and sliding speed on the morphology of surface scratching in abrasive or erosive processes, *Tribol. Int.*, 17(1) (1984) 35-38.
35. B.Y. Du, M.R. Vanlandingham, Q.L. Zhang, T.B. He, Direct measurement of plowing friction and wear of a polymer thin film using the atomic force microscope, *J. Mater. Res.* 16(5) (2001) 1487-1492.
36. E. Hamada, R. Kaneko, Micro-tribological evaluations of a polymer surface by atomic force microscopes, *Ultramicroscopy* 42-44 Part A (1992) 184-190.
37. Y.C. Han, S. Schmitt, K. Friedrich, Nanoscale indentation and scratch of short carbon fiber reinforced PEEK/PTFE composite blend by atomic force microscope lithography, *Appl. Compos. Mater.* 6(1) (1999) 1-18.

38. P. Bertrand-Lambotte, J.L.Loubet , C.Verpy , S.Pavan, Understanding of automotive clearcoats scratch resistance, *Thin Solid Films* 420-421 (2002) 281-286.
39. V. Jardret, H. Zahouani, J.L. Loubet, T.G. Mathia, Understanding and quantification of elastic and plastic deformation during a scratch test, *Wear* 218 (1998) 8-14.
40. S.R. Kim, J.S. Song, Y.J. Choi, J.H. Kim, Preparation of hard coatings on polycarbonate substrate by high frequency ion beam deposition using CH₄/H₂ gases, *Mater. Res. Soc. Symp. – Proc.* 504 (1997) 265-270.
41. L. Lin, G.S. Blackman, R.R. Matheson, Micro-mechanical characterization of mar behavior of automotive topcoats: micro- and nano- wear of polymeric materials, American Chemical Society, *Polymer Preprints, Division of Polymer Chemistry* 39(2) (1998) 1224-1225.
42. A.C.-M. Yang, T.W. Wu, Abrasive wear and craze breakdown in polystyrene, *J. Mater. Sci.* 28 (1993) 955-962.
43. P. Leroux, A. Raveh, J.E., L. Martinu, Mechanical properties of plasma deposited functional coatings determined by microscratch measurements, *Proceedings, Annual Technical Conference – Society of Vacuum Coaters* (1993) 472-477.
44. Micro Photonics Inc., Micro Scratch Tester (MST), July 2003, <http://www.microphotonics.com/mst.html>.
45. CSM Nano Scratch Tester (NST), July 2003, <http://www.microphotonics.com/nst.html>.
46. MTS Systems Corporation, Nano Indenter[®] XP, July 2003, http://www.mts.com/nano/nano_indenter_xp.htm.
47. MTS Systems Corporation, New Nano Indenter[®] XPW, July 2003, <http://www.mts.com/nano/xpw.htm>.
48. Hysitron Inc., TriboIndenter[®] Nanomechanical Test Instrument, July 2003 http://www.hysitron.com/docs/sell%20sheets/new_triboindenter.htm.

49. A. Strojny, X. Xia, A. Tsou, W. W. Gerberich, Techniques and considerations for nanoindentation measurements of polymer thin film constitutive properties, *J Adhesion Sci. Technol.*, 12 (12) (1998) 1299-1321.
50. F.P Bowden, D. Tabor, *The Friction and Lubrication of Solids Part I*, Oxford University Press, Oxford, 1950.
51. A.G. Atkins, Y-W. Mai, *Elastic and Plastic Fracture – metals, polymers, ceramics, composites, biological materials*, Ellis Horwood Ltd, Chichester, 1985.
52. M. Wong, G.T. Lim, A. Moyse, J.N. Reddy, H.J. Sue, A new scratch test methodology for polymers, *Wear* – submitted in May 2003.
53. K. Li, B. Y. Ni, J.C.M. Li, Stick-slip in the scratching of the styrene-acrylonitrile copolymer, *J. Mater. Res.* 11 (1996) 1574-1580.
54. J.A. Williams, Analytical models of scratch hardness, *Tribol. Intern.* 29(8) (1996) 675-694.
55. V. Jardret, B.N. Lucas, W. Oliver, A.C. Ramamurthy, Scratch durability of automotive clear coatings: a quantitative, reliable and robust methodology, *J. Coatings Technol.* 72 (2000) 79-88.
56. P. Rangarajan, M. Sinha, V. Watkins, K. Harding, Scratch visibility of polymers measured using optical imaging, *Polym. Eng. Sci.* 43 (2003) 749-758.
57. Atlas Material Testing Technology, VIEEW[®] Digital Image Analyzer, July 2003, <http://www.atlasmtt.de/cgi-atlas/show.cgi?productid=19&from=digital>.
58. H. Breuer, F. Haaf and J. Stabenow, Stress whitening and yielding mechanism of rubber-modified PVC, *J. Macromol. Sci.— Phys.* B14 (1977) 387-417.
59. J. Holoubek, M. Raab, Stress whitening in polypropylene. I. light scattering theory and model experiments, *Collect. Czech. Chem. Commun.* 60 (1995) 1875-1887.
60. B. J. Briscoe, E. Pelillo, S. K. Sinha, Characterisation of the scratch deformation mechanisms for poly(methylmethacrylate) using surface optical reflectivity, *Polym Intern* 43 (1997) 359-367.

61. C. Xiang, H.-J. Sue, J. Chu, B. Coleman, Scratch behaviour and material property relationship in polymers, *J. Polym. Sci. Polym. Phys.* 39 (2001) 47-59.
62. Polymer Technology Center, Scratch Consortia, July 2003, <http://ptc.tamu.edu/Scratchconsortia.html>.
63. H. Kita, M. Ishiki, M. Maki, T. Kitamura, T. Kuriyama, Scratch behaviors of moldings, *ANTEC 2003 3* (2003) 2992-2996.
64. ASTM D 618-00.
65. M. Kotaki, M. Wong, C. Xiang, H.-J. Sue, Scratch behavior of polypropylene-based blends, *ANTEC 2002 2* (2002) 1535-1539.
66. J.N. Reddy, *An Introduction to the Finite Element Method*, 2nd Ed. McGraw-Hill, New York, 1993.
67. ABAQUS, Inc., *ABAQUS/Explicit Version 6.3*, 1-3 (2002).
68. G.T. Lim, M. Wong, A. Moyse, J.N. Reddy, H.-J. Sue, Mechanical modeling and experimental observation of surface damage phenomena of polymers, *SPE International Conference on Polyolefins* (2003) 577-584.
69. M. Wong, G.T. Lim, P.R. Rood, A. Moyse, J.N. Reddy, H.J. Sue, Scratch damage phenomena of polyolefin materials, *TPO 2003*, (2003) – to be published.
70. A. Dasari, J. Rohrmann, R.D.K. Misra, Micro- and nanoscale evaluation of scratch damage in poly(propylene)s, *Macromol. Mater. Eng.* 287 (2002) 889-903.
71. H. Tang, D. C. Martin, Near-surface deformation under scratches in polypropylene blends Part I Microscopic characterization of deformation, *J. Mater. Sci.*, 38 (2003) 803- 815.
72. C. Pistor, K. Friedrich, Scratch and indentation tests on polyoxymethylene (POM), *J. Applied Polym. Sci.* 66 (1997) 1985-1996.
73. D. Rats, V. Hajek, L. Martinu, Micro-scratch analysis and mechanical properties of plasma-deposited silicon-based coatings on polymer substrates, *Thin Solid Films* 340 (1999) 33-39.
74. N.G. McCrum, C. P. Buckley and C. B. Bucknall, *Principles of Polymer Engineering* 2nd Edition, Oxford Science Publications, Oxford, 1999.

75. R. Rengarajan, S.K. Kesavan, K. L. Fullerton, S. Lee, Ethylene-methacrylic acid copolymers as stress whitening suppressants in polypropylenes, *J Appl. Polym. Sci*, 45 (1992) 317-331.
76. L. Lin, G.S. Blackman, R.R Matheson, in: V.V. Tsukruk, K.L. Wahl, (Eds.), *Microstructures and Microtribology of Polymer Surfaces*, ACS, Washington D.C., pp, 428-438, 2000.

VITA

Min Hao Wong was born and raised in Singapore. He had served in the Singapore Armed Forces for two and a half years before he attended Nanyang Technological University in July 1997, where he studied materials engineering. He completed two research projects. The first project investigated the effect of mechanical deformation on BPSCCO superconductor tape. The second project characterized the properties of carbon nanotubes-polystyrene composite rods which led to a publication in the renowned scientific journal, *Polymer*. Min Hao also completed a 6-month internship with DSO National Laboratories, the foremost defense research and development institute in Singapore. Upon graduation in July 2001, Min Hao furthered his studies at Texas A&M University, where he did his graduate work in the Department of Mechanical Engineering under the supervision of Dr. Hung-Jue Sue. He received his M.S degree in mechanical engineering in the summer of 2003. His permanent address is 506B Serangoon North Ave 4 Apt 14-428, Singapore 552506.